European Journal of Medicinal Chemistry 248 (2023) 115038

Contents lists available at ScienceDirect

European Journal of Medicinal Chemistry

journal homepage: www.elsevier.com/locate/ejmech

Research paper

Investigation of morpholine isosters for the development of a potent, selective and metabolically stable mTOR kinase inhibitor

Martina De Pascale [a,1], Lukas Bissegger [a,1], Chiara Tarantelli [b], Florent Beaufils [a], Alessandro Prescimone [c], Hayget Mohamed Seid Hedad [a], Omar Kayali [b], Clara Orbegozo [a], Luka Raguž [a], Thorsten Schaefer [a], Paul Hebeisen [a], Francesco Bertoni [b,d], Matthias P. Wymann [a,**], Chiara Borsari [a,2,*]

[a] University of Basel, Department of Biomedicine, Mattenstrasse 28, 4058, Basel, Switzerland
[b] Institute of Oncology Research, Faculty of Biomedical Sciences, USI, Via Francesco Chiesa 5, 6500, Bellinzona, Switzerland
[c] University of Basel, Department of Chemistry, Mattenstrasse 24a, 4058, Basel, Switzerland
[d] Oncology Institute of Southern Switzerland, Ente Ospedaliero Cantonale, Bellinzona, Switzerland

ARTICLE INFO

Keywords:
Mechanistic target of rapamycin (mTOR)
mTOR kinase inhibitors
ATP-competitive inhibitors
Morpholine isosters
Metabolic stability
Cancer

ABSTRACT

Upregulation of mechanistic target of rapamycin (mTOR) signaling drives various types of cancers and neurological diseases. Rapamycin and its analogues (rapalogs) are first generation mTOR inhibitors, and selectively block mTOR complex 1 (TORC1) by an allosteric mechanism. In contrast, second generation ATP-binding site inhibitors of mTOR kinase (TORKi) target both TORC1 and TORC2. Here, we explore 3,6-dihydro-2*H*-pyran (DHP) and tetrahydro-2*H*-pyran (THP) as isosteres of the morpholine moiety to unlock a novel chemical space for TORKi generation. A library of DHP- and THP-substituted triazines was prepared, and molecular modelling provided a rational for a structure activity relationship study. Finally, compound **11b** [5-(4-(3-oxa-8-azabicyclo[3.2.1]octan-8-yl)-6-(tetrahydro-2*H*-pyran-4-yl)-1,3,5-triazin-2-yl)-4-(difluoromethyl)pyridin-2-amine] was selected due its potency and selectivity for mTOR kinase over the structurally related class I phosphoinositide 3-kinases (PI3Ks) isoforms. **11b** displayed high metabolic stability towards CYP1A1 degradation, which is of advantage in drug development. After oral administration to male Sprague Dawley rats, **11b** reached high concentrations both in plasma and brain, revealing an excellent oral bioavailability. In a metabolic stability assay using human hepatocytes, **11b** was more stable than PQR620, the first-in-class brain penetrant TORKi. Compound **11b** also displayed dose-dependent anti-proliferative activity in splenic marginal zone lymphoma (SMZL) cell lines as single agent and when combined with BCL2 inhibition (venetoclax). Our results identify the THP-substituted triazine core as a novel scaffold for the development of metabolically stable TORKi for the treatment of chronic diseases and cancers driven by mTOR deregulation and requiring drug distribution also to the central nervous system.

1. Introduction

Mechanistic target of rapamycin (mTOR) is a serine/threonine protein kinase which is a key regulator of lipid and protein synthesis, cytoskeleton rearrangements, cell survival, and cell cycle progression. mTOR kinase is integrated in two functionally non-redundant multiprotein complexes, dubbed mTOR complex 1 (TORC1) and mTOR complex 2 (TORC2) [1]. The mTOR kinase activation cascade usually starts with the recruitment of class IA phosphoinositide 3-kinase (PI3K) to phosphorylated cell surface receptors or their substrates, which initiates the production of PtdIns(3,4,5)P_3 [1,2]. The latter serves as a docking site for protein kinase B (PKB/Akt) and protein 3-phosphoinositide-dependent protein kinase-1 (PDPK1/earlier dubbed PDK1). To be fully active, PKB/Akt must be phosphorylated at Thr308 by PDPK1 and

* Corresponding author.
** Corresponding author.
E-mail addresses: matthias.wymann@unibas.ch (M.P. Wymann), chiara.borsari@unibas.ch (C. Borsari).
[1] M.D.P. and L.B. contributed equally to this work.
[2] Current address: University of Milan, Department of Pharmaceutical Sciences, Via Mangiagalli 25, 20133 Milan, Italy. Email: chiara.borsari@unimi.it

https://doi.org/10.1016/j.ejmech.2022.115038
Received 28 September 2022; Received in revised form 17 December 2022; Accepted 18 December 2022
Available online 28 December 2022

at Ser473 by TORC2 and other hydrophobic motif kinases [3,4]. Activation of S6 kinase (S6K) by TORC1 results in the phosphorylation of the downstream effector ribosomal protein S6 (S6) and eukaryotic translation initiation factor 4E-binding protein (4E-BP1). Phosphorylation of S6K or S6 are reliable readouts for mTORC1 activity [5]. The main negative regulator of mTORC1 is the tuberous sclerosis complex (TSC) complex formed by hamartin (TSC1) and tuberin (TSC2). PKB/Akt phosphorylates TSC2 to disrupt the TSC1/2 complex, which releases TORC1 activation.

mTOR activity is altered in a number of human disorders such as cancer, diabetes, obesity, and genetic disorders [3,6]. Inhibitors targeting mTOR kinase are evaluated as therapeutic agents in advanced solid tumors and haematological malignancies [7,8]. In addition, dysregulation of the mTOR signaling pathway has been linked to the pathogenesis of a variety of neurological diseases, including neurodegenerative disorders such as Alzheimer's, Parkinson's and Huntington's disease [9].

Rapamycin and its semi-synthetic analogues (rapalogs) are first-generation mTOR inhibitors and are potent, allosteric inhibitors of mTORC1. They bind simultaneously to FK506-binding protein 12 (FKBP12) and the FKBP−rapamycin-binding (FRB) domain of mTOR and thus initiate the formation of a TORC1/rapalog/FKBP12 complex [10]. Rapamycin (Sirolimus) has been successfully used as immunosuppressive agent after organ transplantation [11], but it also halts tumor growth. Rapalogs, including everolimus (RAD001) and temsirolimus (CCI-779), have improved pharmaceutical properties, including stability and solubility, with respect to rapamycin (see Fig. 1A for chemical structures) [12]. Temsirolimus, a synthetic rapamycin ester, has received approval by both the Food and Drug Administration (FDA) and the European Medicines Agency for patients with high-risk, advanced renal cell cancer and with mantle cell lymphoma [13]. Everolimus has been approved for multiple indications in oncology [14]. Nevertheless, the efficacy of rapalogs as single-agents in cancer treatment has been limited by dangerous immunosuppressive adverse effects [15]. Recently, a novel chemical strategy has been proposed to minimize systemic adverse effects of rapalogs, while targeting TORC1 in the brain [16,17].

Second generation mTOR inhibitors target the ATP-binding pocket of mTOR kinase and block the activity of both TORC1 and TORC2 [18]. The clinically most advanced ATP-competitive mTOR kinase inhibitors (TORKi) are sapanisertib (INK128, MLN0128, TAK-228) [19], onatasertib (CC-223, ATG-008) [20] and vistusertib (AZD2014, Fig. 1B) [21]. In 2022, sapanisertib has received FDA fast track approval for patients with advanced non-small cell lung cancer (NSCLC) [22]. ATG-008 is currently investigated in multiple clinical trials for patients with hepatocellular carcinoma (HCC) [23] and lymphomas [www.clinicaltrials.gov]. AZD2014 entered multiple clinical trials for the treatment of hard-to-treat cancers; however, AstraZeneca seems to have discontinued its clinical development.

Beside the clinical candidates above, TORKi covering a wide chemical space have been developed and investigated in preclinical studies for the treatment of cancer and neurological disorders. These scaffolds include triazines [25,26], thienopyrimidines [27], thiazolopyrimidines, purines [28], tricyclic pyrimido-pyrrolo-oxazines [29–31], and pyrazolo [3,4-*d*]pyrimidines [32] (for a review see Ref. [18]).

In 2018, we discovered PQR620 (Fig. 1C), the first-in-class, highly selective ATP-competitive mTOR inhibitor crossing the blood brain barrier (BBB) with the potency to attenuate epileptic seizures in a mouse model of Tuberous Sclerosis Complex (TSC) [26]. PQR620 is well suited for the exploration of mTOR function in rodents due to its metabolic stability in rat and mouse, and has been used as chemical probe to deconvolute the effect of ATP-competitive TORKi in treatment of epilepsy [33], Huntington disease [34], and for decreasing the incidence of seizures induced by a CNS-specific deletion of TSC1 [35]. Moreover, PQR620 has been investigated as anti-cancer agent in mouse models of non-small cell lung cancer [36] and lymphoma [37]. Despite promising results in rodent disease models, the limited stability of PQR620 in human hepatocyte assays and short half-live in PK studies in Cynomolgus monkeys [25] with a high predictable value for drug turnover in humans, prevented its entry into clinical development for oncology applications. PQR620 is still a candidate for topical applications and for the treatment of disorders where a short half-life – to reduce systemic exposure – can be beneficial.

Recently, we have discovered PQR626 (Fig. 1C), a TORKi displaying an improved stability in human hepatocytes compared to PQR620 [25]. Aiming to develop a follow-up compound for PQR620 and PQR626, we investigated the 3,6-dihydro-2*H*-pyran (DHP) and the tetrahydro-2*H*-pyran (THP) as isosteres of the morpholine moiety. The DHP and THP rings are not extensively explored substitutions compared to the morpholine privileged scaffold. While more than 100 marketed drugs contain a morpholine ring [38], the DHP and THP motifs have been explored only recently in drug discovery [39,40]. Successful replacements of the morpholine ring with DHP have been reported for aryl-substituted pyrazolopyrimidines and thienopyrimidines [41], and

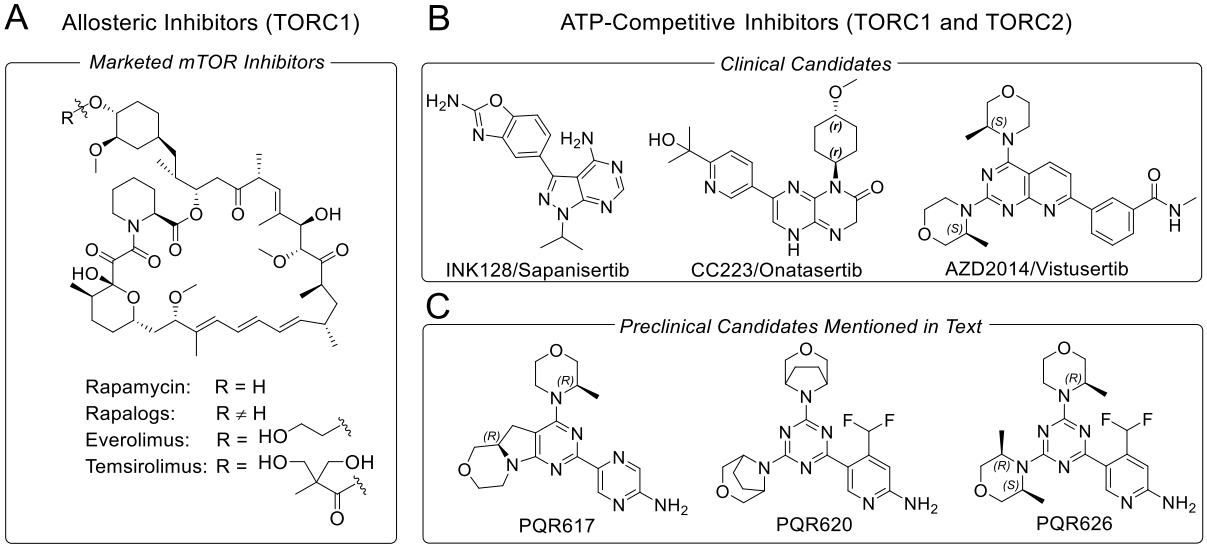

Fig. 1. Chemical structures of mTOR inhibitors. (A) Rapamycin and its synthetic analogues (rapalogs) form a TORC1-rapalog-FKBP12 complex and inhibit TORC1 allosterically [10,24]. (B, C) Chemical structure of TORKi clinical candidates (B) and selected preclinical candidates mentioned in text (C).

pyrimidine-containing TORKi [42]. Indeed, the DHP moiety appended to pyrazolopyrimidines and thienopyrimidines led to potent mTOR inhibitors (IC_{50} in the low nanomolar range) [41]. However, DHP has not been introduced on the triazine scaffold yet, and the THP ring has not been reported in any effective TORKi. On the pyrazolo[3,4-*d*]pyrimidine core, the introduction of the fully saturated tetrahydropyran (THP) led to inactivity toward mTOR kinase [41]. Here, we present first-in-class TORKi bearing a THP motif and reveal the binding mode to mTOR kinase. We assessed the metabolic stability of the novel, selective ATP-competitive TORKi (**11b**) in human hepatocytes in comparison with PQR620. The antiproliferative activity in lymphoma cell lines, paired with the brain permeability, characterized **11b** as a promising candidate to be further investigated in oncology.

2. Chemistry

A library of triazine derivatives was designed and prepared as reported in Scheme 1. Compounds **1a-6a** were synthesized starting from 2,4-dichloro-6-(morpholin-4-yl)-1,3,5-triazine [43] (**12**) *via* consecutive palladium catalyzed Suzuki cross-coupling reactions: First, the DHP moiety was introduced by 3,6-dihydro-2*H*-pyran-4-boronic acid pinacol ester (**18**, 57% yield), followed by the displacement of the chlorine of the intermediate **18** by selected heteroaromatic rings Ar_n (Ar_0–Ar_5), using the respective boronic ester (see Experimental Part for details). Compounds **1a-6a** were then reduced with hydrogen over a palladium on carbon catalyst to afford the THP derivatives **1b-6b** in moderate to good yields (23–70%, Scheme 1A).

Dichlorotriazine intermediates **13–17** were prepared from cyanuric chloride *via* nucleophilic aromatic substitution (S_NAr) with piperidine M_1 or substituted morpholines M_n (M_2-M_5; Scheme 1B), namely 3-methylmorpholine [M_2: (*R*) and M_3: (*S*)], (3*S*,5*R*)-dimethylmorpholine (M_4) and 3-oxa-8-azabicyclo[3.2.1]octane (M_5). Depending on the morpholine substituent, the Suzuki cross-coupling reaction with 3,6-dihydro-2*H*-pyran-4-boronic acid pinacol ester yielded the desired intermediates

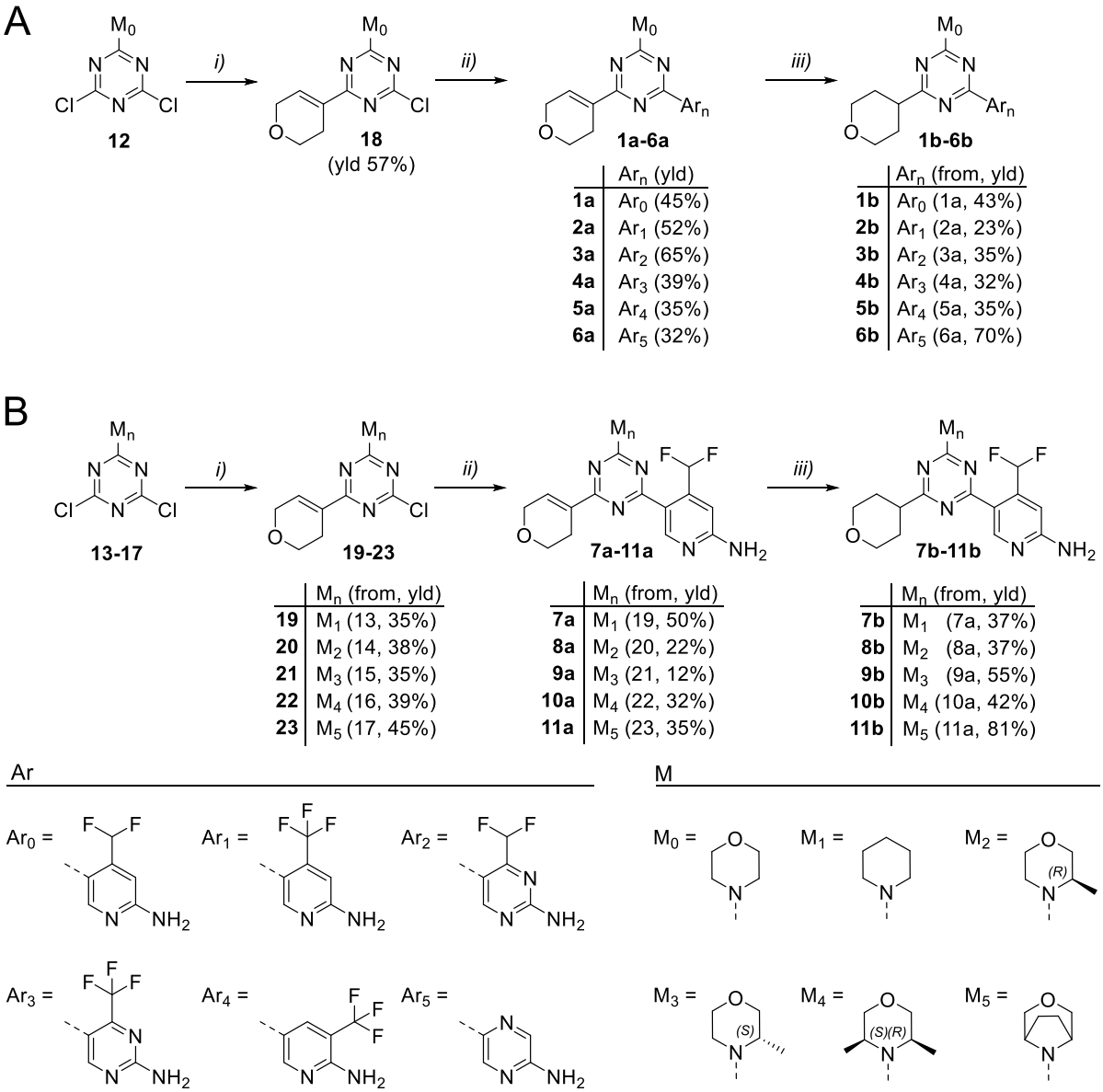

Scheme 1. Synthesis of the SAR library. (A) Preparation of **1a-6a** (DHP derivatives), and **1b-6b** (THP derivatives) bearing a variety of heteroaromatic rings. (B) Preparation of **7a-11a** (DHP derivatives) and **7b-11b** (THP derivatives) bearing different morpholines (**8a-11a** and **8b-11b**) or piperidine (**7a** and **7b**). Reagents and conditions: (i) 3,6-dihydro-2*H*-pyran-4-boronic acid pinacol ester, $Pd(dppf)Cl_2$ (cat.), K_3PO_4, dioxane/H_2O, 85 °C, 5 h; (ii) 1) boronic ester **24**, XPhosPdG2 (cat.), K_3PO_4, dioxane/H_2O, 95 °C, 2–15 h; 2) HCl, H_2O, 80 °C, 3 h; (iii) Pd/C (cat.), MeOH, 25–40 °C, 24–72 h.

19–23 in moderate yields (35–45%). The subsequent coupling reaction with boronic ester **24** gave compounds **7a-11a** in low to moderate yields (12–50%). The last synthetic step involved the palladium catalyzed hydrogenation of the unsaturated pyran ring to obtain the corresponding tetrahydropyran derivatives **7b-11b** in 37–81% yields.

3. Results and discussion

3.1. SAR study: investigation of in vitro and cellular activity

We selected the triazine core as central scaffold since this six-membered heterocycle is considered a privileged building block and our extensive knowledge on triazine-containing TORKi. Here, we investigated the effect of replacing the morpholine (ML) with either DHP or THP on the cellular and *in vitro* activity. Three heteroaromatic rings, pyridine, pyrimidine and pyrazine (Ar_n, Scheme 1A), were introduced for scaffold exploration optionally substituted with difluoromethyl- and trifluoromethyl groups. The library was evaluated for the *in vitro* activity towards mTOR and PI3Kα, and for the ability to inhibit the PI3K-mTOR axis in SKOV3 cells (see Material and Methods for assay conditions). The morpholine-substituted triazines bearing the DHP and THP moieties maintained an analogue selectivity profile of dimorpholine-substituted triazines, highlighting that affinity was driven by the accommodation of the heteroaromatic ring into the binding affinity pocket of the kinases, while selectivity was guided by the substitutions on the hinge region-binding morpholines (see Table 2 and paragraph 3.2). The presence of a CHF_2-pyridine led to dual mTOR/PI3Kα inhibitors [K_i(mTOR) **1a** and **1b** = 66, 34 nM; K_i(p110α) **1a** and **1b** = 38, 39 nM], while CF_3-pyridine derivatives (**2a** and **2b**) resulted in PI3Kα inhibitors with moderated mTOR activity [K_i(p110α) **2a** and **2b** = 25, 56 nM; K_i(mTOR) **2a** and **2b** = 107, 148 nM]. Both the difluoromethyl- and trifluoromethyl-substituted substituted pyrimidines (**3a**/**3b** and **4a**/**4b**, respectively) displayed selective PI3Kα inhibition (selectivity K_i(p110α)/K_i(mTOR) between 0.011 and 0.17-fold, Table 1). The 3-CF_3-substituted pyridine and pyrazine were introduced as they provided an excellent mTOR selectivity on the conformationally restricted tricyclic pyrimido-pyrrolo-oxazine scaffold [29,30]. However, when appended on the dimorpholine-substituted triazine scaffold, these two heteroaromatic moieties led to inactive derivatives [44]. As expected the same trend was observed for THP- and DHP-substituted molecules (**5a**/**5b** and **6a**/**6b**),

Table 1
SAR study on the heteroaromatic ring exploration.

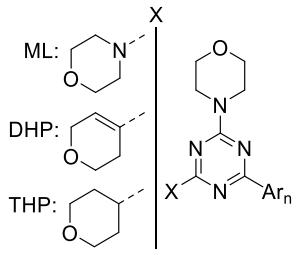

Name	Ar_n		Cellular Activity IC_{50} [nM][a]		*in vitro* Binding Assays K_i [nM][b]		Selectivity K_i(p110α)/K_i(mTOR)	clogP[c]	PSA[c]
			pPKB S473	pS6 S235/236	p110α	mTOR			
PQR411[d]	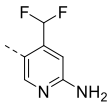	ML	73	52	12	6.9	1.7	2.07	102.5
1a		DHP	82	187	38	66	0.57	3.30	99.3
1b		THP	75	112	39	34	1.1	2.94	99.3
PQR309[d]		ML	97	81	17	62	0.27	2.72	102.5
2a		DHP	73	227	25	107	0.23	4.02	99.3
2b		THP	178	306	56	148	0.38	3.66	99.3
PQR514[d]	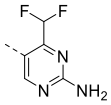	ML	45	36	2.2	33	0.067	1.58	115.4
3a		DHP	130	487	8.1	422	0.019	2.75	112.2
3b		THP	82	204	21	119	0.17	2.40	112.2
PQR127[d]		ML	206	197	8.1	203	0.040	2.36	115.4
4a		DHP	156	443	22	1920	0.011	3.58	112.2
4b		THP	183	485	46	329	0.14	3.22	112.2
5a	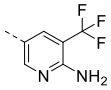	DHP	>3000	>3000	1270	411	3.09	4.02	99.3
5b		THP	>3000	>3000	938	160	5.86	3.66	99.3
6a	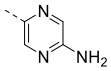	DHP	>3000	>3000	1179	3089	0.38	2.22	112.2
6b		THP	>3000	>3000	1138	1093	1.04	1.87	112.2

[a,b]The *in vitro* and cellular assays have been performed as reported in Refs. [25,29].

[a] The phosphorylation of protein kinase B (pPKB, pSer473) and ribosomal S6 (pS6, pSer235/236) were determined in SKOV3 cells exposed to listed compounds. Phosphoproteins were quantified with an in-cell western (ICW) assay described in section 5.4.5. IC_{50}s were calculated from 11-point 1:2 serial compound dilutions performed in independent experiments (n = 2, mean ± SD [standard errors are reported with Log IC_{50}s in Table S1 in the Supporting Information]).

[b] Compounds' dissociation constants (K_i) for the ATP-binding pocket of PI3Kα and mTOR were determined using a time-resolved FRET (TR-FRET) assay described in Ref. [43]. TR-FRET IC_{50}s were calculated from 10-point 1:4 serial dilutions (n = 2). The IC_{50} to K_i conversion factor was determined based on tracer 314-binding curves to p110α and mTOR kinase and was 9.84 and 2.05, respectively. The calculated IC_{50} and K_is values are in Table S1, displayed as mean ± SD.

[c] Marvin/JChem 20.9 was used to predict partition coefficient (clogP) and polar surface area (PSA); ChemAxon (https://www.chemaxon.com).

[d] *In vitro* data for PQR411, PQR309, PQR514 and PQR127 are from Ref. [47].

Table 2
Exploration of substituted morpholines on DHP- and THP-substituted triazines.

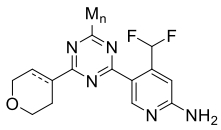

Name	M_n		Cellular Activity IC_{50} [nM][a]		*in vitro* Binding Assays K_i [nM][b]		Selectivity K_i(p110α)/K_i(mTOR)	clogP[c]	PSA[c]
			pPKB S473	pS6 S235/236	p110α	mTOR			
1a		DHP	82	187	38	66	0.57	3.30	99.3
1b		THP	75	112	39	34	1.1	2.94	99.3
8a		DHP	235	71	281	48	5.9	3.71	99.3
8b		THP	234	73	1014	82	12	3.36	99.3
9a		DHP	85	35	28	29	0.97	3.71	99.3
9b		THP	60	19	29	42	0.68	3.36	99.3
10a		DHP	103	52	53	16	3.3	4.13	99.3
10b		THP	195	111	67	38	1.8	3.77	99.3
11a		DHP	199	94	125	16	7.8	3.77	99.3
11b		THP	171	85	1135	22	52	3.41	99.3

Indexes [a,b,c] correspond to assignments in legend of Table 1.

which were inactive towards both mTOR and PI3Kα (Table 1). For the whole SAR, the *in vitro* data matched the cellular results in SKOV3, revealing a good cellular permeability as also expected from the clogP values. The bioisosteric replacement of the morpholine moiety with a DHP or THP motif also influenced the physicochemical properties of the resulting compounds: **1a** and **1b** presented a lower polar surface area (PSA) than their morpholine analog (PQR411; Table 1). For good brain penetration of CNS drugs, PSA should be < 100 $Å^2$, or even smaller <60–70 $Å^2$ [45,46].

The CHF_2-pyridine was selected for further SAR studies as it led to DHP- and THP-substituted derivatives with good affinity for mTOR kinase (see compounds **1a** and **1b**). We synthesized a library of compounds bearing piperidine (M_1) and a variety of substituted morpholines (Scheme 1B, M_n substituents), including 3-methylmorpholine [M_2: (*R*) and M_3: (*S*)], (3*S*,5*R*)-3,5-dimethylmorpholine (M_4), and 3-oxa-8-azabicyclo[3.2.1]octane (M_5). M_1 (compounds **7a** and **7b**) was introduced to elucidate the binding mode (see next paragraph for an explanation of binding modes), while M_2-M_5 were selected as they are known to bind in the hinge region of mTOR kinase. Whereas **1a** and **1b** bearing an unsubstituted morpholine were dual mTOR/PI3Kα inhibitors, the presence of (*R*)-3-methylmorpholine (compounds **8a** and **8b**) led to preference for mTOR kinase activity, with the THP derivative **8b** being the most selective molecule [K_i(p110α)/K_i(mTOR) ratio of 5.9 for **8a**, and of 12 for **8b**; Table 2]. According to previous studies, the (*R*)-3-methylmorpholine, binding to the mTOR hinge region, is able to confer selectivity for mTOR kinase over the structurally related PI3Ks [25,28,48]. In cancer cells, **8a** and **8b** displayed good activity (IC_{50} for S6 phosphorylation was 71 nM for **8a** and 73 nM for **8b**). Introduction of a (*S*)-3-methylmorpholine on the DHP- and THP-substituted triazine led to potent, dual mTOR/PI3Kα inhibitors [K_i(mTOR) **9a** and **9b** = 29, 42 nM; K_i(p110α) **9a** and **9b** = 28, 29 nM], as previously described for the morpholine-substituted triazine PQR530 [49] (see Supporting Information for chemical structure). The dual mTOR/PI3Kα inhibition by **9a** and **9b** resulted in excellent cellular potency [IC_{50}(pPKB/Akt) = 85 and 60 nM, and IC_{50}(pS6) = 35 and 19 nM, respectively]. Replacement of (*S*)-3-methylmorpholine with (3*S*,5*R*)-3,5-dimethylmorpholine (compounds **10a** and **10b**) allowed to maintain strong affinity for mTOR (K_i **10a** and **10b** = 16, 38 nM), but slightly decreased the potency for PI3Kα (K_i of 53 nM for **10a**, and of 67 nM for **10b**). This also led to a decrease in cellular activity (see **9a/9b** vs **10a/10b**, Table 1). The introduction of sterically demanding morpholines had been previously described as a chemical strategy to gain mTOR selectivity for different TORKi scaffolds [26,32]. The installation of a bulky 3,5-ethylene bridged morpholine on a morpholine-substituted triazine core (PKI-179, see Supporting Information for chemical structure) did not result in mTOR-selective inhibition, as the unsubstituted morpholine is well accommodated in the hinge region of both mTOR and PI3Ks [50]. In contrast, a highly potent and selective TORKi was obtained by introducing two sterically hindered morpholines on the triazine core (PQR620, Fig. 1C). Therefore, we introduced the 3-oxa-8-azabicyclo[3.2.1]octane (M_5, Scheme 1B) on our novel DHP- and THP-substituted triazines to dial out PI3K, as the DHP and THP oxygen cannot establish the pivotal hydrogen bond with the backbone valine residue at the hinge region of mTOR and PI3K (see paragraph 3.2). Compound **11a**, bearing a DHP moiety, was 8 times more selective for mTOR kinase with respect to PI3Kα [K_i(mTOR) = 16 nM and K_i(PI3Kα) = 125 nM]. The THP derivative **11b** showed a 56-fold selectivity for mTOR, resulting the most selective TORKi among this compound library [K_i(mTOR) = 22 nM and K_i(PI3Kα) = 1135 nM]. Its high mTOR affinity resulted also in a good cellular potency (IC_{50} for pS6 = 85 nM), leading to the selection of **11b** as a cell permeable TORKi for further investigation.

3.2. Computational studies for binding mode elucidation

To elucidate the binding mode of DHP- and THP-substituted triazines, we performed modelling studies to reveal the inhibitor binding modes into the ATP-binding pocket of the kinases. As reported in literature for morpholino-substituted mTOR and PI3K inhibitors [2,25,49,51], the morpholine oxygen atom forms a pivotal H-bond with the backbone amide of the hinge region valine (Val2240 in mTOR and Val851 in PI3Kα). First, we investigated whether the DHP and THP

moieties could bind to the kinase hinge region. We started from the X-ray crystallographic complex [52] of mTOR and PI103 (PDB ID: 4JT6, resolution: 3.6 Å) and substituted the original ligand with PQR411, compounds **1a** and **1b** (Table 1). The mTOR-PI103 complex (PDB ID: 4JT6) was selected as starting point for model generation as PI103 has the highest structural similarity with our compound class. PI103 is the only morpholine-substituted mTOR inhibitor that has been co-crystallized with mTOR, representing the most suited ligand to be replaced by our morpholine-based compounds. The other X-ray crystallographic structures (PDB ID: 4JSX and 4JT5) accommodate inhibitors lacking the morpholine moiety pointing toward the hinge region Valine, thus their binding mode cannot resemble that of compounds bearing a morpholine ring. We performed energy minimization and confirmed that the complexes of mTOR with our inhibitors maintained the H-bond between the unsubstituted-morpholine O-atom and the backbone NH of Val2240 (Fig. 2A). The morpholine ring and the triazine core of PQR411 were quasi co-planar due to stabilizing electronic overlap between the morpholine nitrogen lone pair and the heteroaromatic ring [42]. In the minimum energy conformation, the DHP ring of **1a** was quasi co-planar with the triazine core, adopting a similar conformation to that of the morpholine-substituted derivative. Even though the DHP oxygen atom was found at a donor-to-acceptor distance for energetically significant H-bond (<3.5 Å), the oxygen lone-pair orbitals of the acceptor atom were displaced from a plane containing the hydrogen atom. Thus, the interaction in the hinge region between the DHP oxygen atom and the valine backbone amide are disfavored (Fig. 2B). Similarly, the key hydrogen bonding interaction with the hinge region was lost for the tetrahydropyran. Indeed, hydrogen-bond vector directionality is an important factor in many hydrogen-bonded structures [53]. The minimum energy conformation for the THP group was rotated approximately 90° out-of-plane with the triazine core (Fig. 2C).

The inability of DHP and THP groups to fit into the hinge region of mTOR and PI3Kα was further confirmed exchanging the unsubstituted morpholine of **1a** and **1b** with piperidine (compounds **7a** and **7b**, respectively, Scheme 1B). **1a** and **1b** showed high affinity for PI3Kα and mTOR, highlighting the ability of the unsubstituted morpholine to accommodate into the hinge region of the ATP-binding pocket of the kinases (Table 3). In contrast, the piperidine-substituted derivatives (**7a** and **7b**) were completely inactive towards mTOR and PI3Kα (K_i for mTOR and for PI3Kα > 800 nM, IC_{50} for pPKB and pS6 > 3000 nM; Table 3). These results show that when DHP and THP are bound in the solvent exposed region, they have a minimal negative influence on binding affinity. The CHF_2-pyridine in the mTOR binding affinity region is the affinity driver, whereas the sterically demanding or (*R*)-methyl-substituted morpholines in the hinge region are guiding selectivity for mTOR.

Likewise, we replaced PI103 in PDB 4JT6 [52] with **11b** to predict its interactions with mTOR. After energy minimization of the resulting mTOR-**11b** complex, we observed that the H-bonds involving the NH_2-pyridine and Glu2190/Asp2195 were maintained. In addition, the oxygen atom of the sterically hindered morpholine established the key H-bond with Val2240 backbone amide. The bulky morpholine fits in the hinge region of mTOR kinase (Fig. 2D), and provides selectivity for mTOR over the structurally related PI3Ks [with a K_i(p110α)/K_i(mTOR) ratio of 56]. Indeed, the 3,5-ethylene bridged morpholine is known to induce steric clashes in the rigid hinge region of PI3K [26]. The proton of the CHF_2-group could either (i) interact with Glu2190, or (ii) form an intramolecular H-bond with a nitrogen of the triazine core (see Fig. 2E). The fully saturated tetrahydropyran of **11b** pointed toward the solvent exposed region and adopted an out of plane conformation (Fig. 2E). The DHP of compound **11a** was co-planar with the triazine core (Fig. 2F), confirming the energy minimization results obtained for **1a** and **1b** (Fig. 2B and C).

3.3. Single-crystal X-ray diffraction of 11a and 11b

X-ray crystallographic studies have been performed for **11a** and **11b** to obtain reliable and precise 3-D structural parameters. Although the connectivity of compounds **11a** and **11b** were very similar as they differed only with respect to the presence (**11a**) or absence (**11b**) of a double bond on the pyran ring (Scheme 1B), their crystal structures displayed remarkable differences (Fig. 3A and B). Compound **11b** was crystallized as hydrochloride resulting in protonation of the pyridine *N* rather than the amino *N* (Fig. 3B). This leads to the formation of a net of hydrogen bonds involving both the N-pyridine and NH_2 group as H-donors and the chloride as acceptor. The torsion between the pyridine and THP to the central triazine core was also significantly different between the two compounds: **11a** displayed a flat structure as the twists between the planes calculated through each ring with the central one was only 5.61(9)° for the DHP and 5.12(7)° for the pyridine ring (Fig. 3A). As also predicted by the modelling studies (see 3.2), the THP was significantly more twisted than the DHP moiety, resulting in torsions of 33.31(16)° for the THP and 40.51(12)° for the pyridine of **11b** (Fig. 3B and Table S2). The torsion of the **11b** CHF_2-pyridine could be related to the presence of the chloride anion that was closely packed to the molecules causing steric hindrance and directing the position of the heteroaromatic ring via the hydrogen bonds (Fig. 3B). On a supramolecular level, **11b** packs in rows arranged in a zig-zag manner along the *b* axis (Fig. 4B).

The crystal structure of **11a** was also defined by the channels that run along the c crystallographic axis that contained the disordered solvent which needed to be taken out of the refinement via the use of a solvent mask (Fig. 4A). This particular arrangement allowed pairs of molecules,

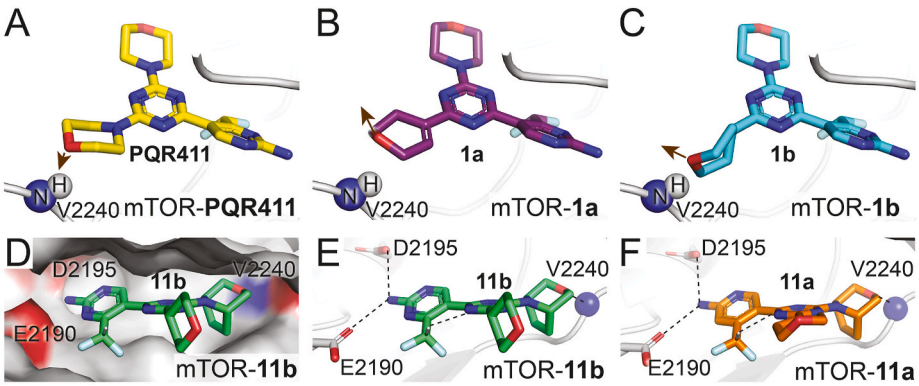

Fig. 2. (A, B, C) Docking of (A) PQR411 (yellow), (B) **1a** (cyan), and (C) **1b** (purple), into mTOR (gray) starting from PDB: 4JT6. Comparison between (A) morpholine, (B) DHP, and (C) THP orientation after energy minimization. The direction of the oxygen lone-pair orbitals is shown as an arrow. Only for the morpholine the oxygen, its lone-pair orbitals of the acceptor atom are in a plane extending to embrace the hydrogen atom, favoring an H-bond. (D, E, F) Docking of **11b** (green in panels D and E), and **11a** (orange in F) into mTOR (gray) starting from PDB: 4JT6. Surface representation is shown to describe the binding mode of **11b** into mTOR (D). The bridge-morpholine accommodates well in mTOR (D) while it induces steric clashes in PI3Ks (see Ref. [26]). Comparison between DHP (E) and THP (F) orientation in the solvent exposed region of mTOR. The hydrogen bonds are shown as dashed black lines. The NH group of Val2240 backbone amide is represented as a sphere.

Table 3
SAR study to elucidate compound binding mode.

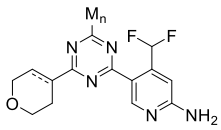

Name	M_n		Cellular Activity IC_{50} [nM][a]		*in vitro* Binding Assays K_i [nM][b]		Selectivity K_i(p110α)/K_i(mTOR)	clogP[c]	PSA[c]
			pPKB S473	pS6 S235/236	p110α	mTOR			
1a		DHP	82	187	38	66	0.57	3.30	99.3
1b		THP	75	112	39	34	1.1	2.94	99.3
7a		DHP	>3000	>3000	1879	896	2.1	4.36	90.1
7b		THP	>3000	>3000	1383	5858	0.24	4.01	90.1

Indexes [a,b,c] correspond to assignments in legend of Table 1.

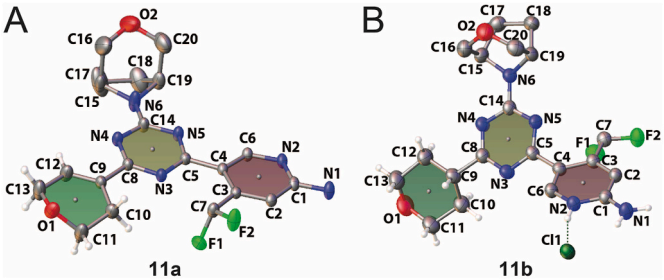

Fig. 3. (A, B) Crystallographic representation of **11a** (A) and **11b** (B). The yellow (triazine), green (DHP and THP) and red (pyridine) planes are the mean planes through the respective rings. For clarity reasons, most of the H atoms are not displayed. The H atoms on the DHP and THP have been placed to highlight the presence or absence of the double bond (see C9–C12 bond). H atoms on the N atom and NH_2 group of the pyridine ring of **11b** were placed to show the protonated N atom (see N2) and its H-bond with the Cl ion. See also Tables S2–S11 of Supporting Information for crystallographic data including coordinates, bond lengths and angles.

generated by the inversion center lying in between them and belonging to adjacent channels, to make π-π staggered stacking between the central rings thus favoring a "flatter" pattern of the molecular environment (Figs. 4A and 3A).

3.4. Investigation of mTOR potency and selectivity

Considering its cellular potency, high affinity and selectivity for mTOR, compound **11b** was further characterized by DiscoverX KdELECT assays, which confirmed the low nanomolar affinity of **11b** for mTOR kinase (K_d: 5 nM). In addition, **11b** was 80 times more selective for mTOR over PI3K isoforms, exceeding the selectivity of sapanisertib [19] (~40 ×, Table 4). Despite its *in vitro* selectivity, sapanisertib is not a selective TORKi at the micromolar concentrations required for cellular experiments and clinical trials (K_d p110α = 15 nM). The selectivity of **11b** for mTOR compared to class I PI3K was comparable to that of onatasertib [20] (Fig. 1), another competitor TORKi. Onatasertib displayed a low nanomolar affinity for the type III phosphatidylinositol 4-kinase beta isoform (PI4Kβ; K_d = 39 nM), which is evolutionarily similar to class I PI3Ks, and is involved in viral infection [54]. PI4Kβ targeting turned out as a promising strategy to eradicate multiple human pathogens, including plasmodium and cryptosporidium [55,56]. In addition, chronic inhibition of PI4Kβ in humans causes immunosuppressive effects [55], and a PI4Kβ inhibitor (UCB9608) has been recently proposed as immunosuppressive agents to prevent allograft rejection

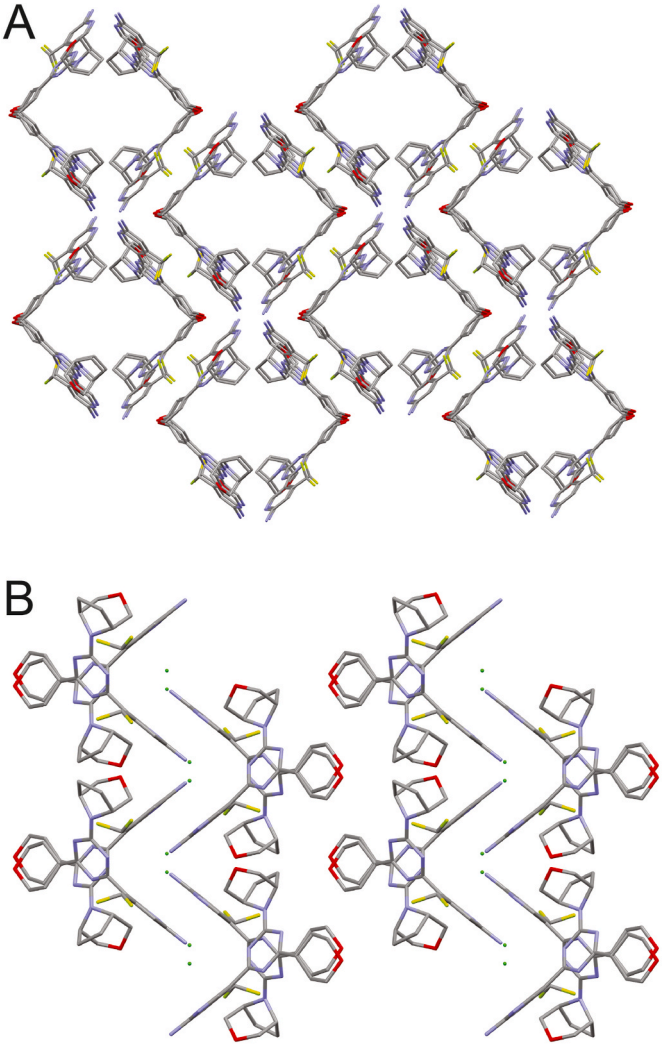

Fig. 4. (A, B) Packing diagrams of **11a** and **11b** as seen along the crystallographic *c* axis. On a supramolecular level, **11a** showed channels and pairs of molecules from adjacent channels (A). For **11b**, a zig-zag alignment of molecules was observed (B). Space group **11a**: *I*2/*a*; **11b**: $P2_1/c$.

Table 4
Binding Affinity of **11b** and Reference Molecules for mTOR and Lipid Kinases.

Kinase →	Inhibitor binding constants[a] K_d, [nM]							*Most sensitive PI3K/mTOR
	mTOR	PI3Kα	PI3Kβ	PI3Kδ	PI3Kγ	PI4Kβ	VPS34	Fold selectivity (Class I PI3K isoforms)
11b	5	**420**	6450	15500	5600	>30000	6100	>80x
Sapanisertib (INK128)[b]	0.092	15	81	30	**3.7**	n.d.	8200	>40x
Onatasertib (CC223)[b]	28	**2300**	18500	6200	7150	39	2500	>80x

[a] Dissociation constants (K_d) were measured by the ScanMax technology from DiscoverX. An 11 point 3-fold serial dilutions of the tested inhibitors were performed. Experiments were carried out in duplicate. K_d values are reported as mean and calculated, using the Hill equation, from the dose response curves.
[b] These data are reprinted from literature, Ref. [29]. n.d. means not determined. *Fold selectivity is calculated as the ratio of K_d for the most sensitive isoform of Class I PI3Ks (shown in bold) compared to the K_d for mTOR.

[57]. Our compound **11b** did not show any PI4Kβ inhibition (K_d > 30000 nM, Table 4), which could lead to immunosuppression.

3.5. Metabolic stability studies and cytochrome P450 reaction-phenotyping

Despite the excellent profile in rodents, PQR620 is known to have a poor stability in human hepatocytes which prevents its entry into clinical development for oncology applications (Table S13 and Ref. [25, 26]). Aiming to reveal a TORKi with improved metabolic stability, compound **11b** was incubated with hepatocytes from CD-1 mice, Sprague-Dawley rats, Beagle dogs, and humans. As previously reported, the hepatocyte stability reflects the variability in *in vivo* clearance among the different species [44]. After incubation with rat and human hepatocytes, **11b** showed a moderate stability, as indicated by 62.4% and 59.9% remaining compound after 3 h of incubation (Fig. 5A). A good stability was observed with mouse hepatocytes (74.5%) and a high stability with dog hepatocytes (92.9%, Fig. 5B and Table S12). Half-lives were >3 h for all species (Table 5). Species differences between rodent and human hepatocytes were minor, as indicated by resulting low-to moderate intrinsic clearance (CL_{int}) rates of 2.1, 3.0 and 3.6 μL/min/10^6 cells, whereas clearance with dog hepatocytes was even lower (0.417 μl/min/10^6 cells, Table 5). Compound **11b** outperformed

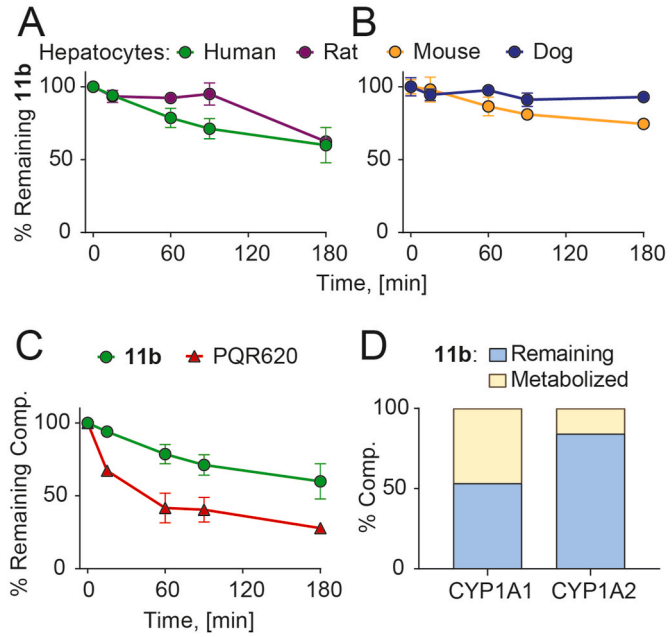

Fig. 5. (A, B) Metabolic stability of **11b** (5 μM) in hepatocytes from humans and rats (A), mice and dogs (B). Experiments were performed in duplicate and data are shown as mean ± SEM. Error bars are not displayed if smaller than the symbols. Exact values are tabulated in Table S12 (C) Comparison between **11b** and PQR620 metabolic stability with human hepatocytes. (D) Stability of **11b** towards CYP1A1 and CYP1A2 metabolism. Incubation time: 60 min.

Table 5
Evaluation of metabolic stability of 11b in hepatocyte cultures, compared to PQR620.

Comp. and species		Mouse	Rat	Dog	Human
11b	[a]CL_{int}	2.11	2.99	0.42	3.56
	$t_{1/2}$ [min]	>180	>180	>180	>180
PQR620[b]	[a]CL_{int}	2.67	1.85	1.65	8.02
	$t_{1/2}$ [min]	>180	>180	>180	108
7-EC[c]	[a]CL_{int}	50	18	45	22
	$t_{1/2}$ [min]	17	47	18	39

[a] Intrinsic clearance (CL_{int}) as μl/min/10^6 cells and half-life ($t_{1/2}$) expressed in minutes.
[b] Values reprinted from Ref. [25].
[c] 7-Ethoxycoumarin (7-EC) was used as assay reference. Experiments were performed in duplicate and data are shown as mean.

the human hepatocytes stability of PQR620 (Fig. 5C), leading to significant advantages for the development of a novel TORKi for potential preclinical and clinical investigation in oncology. In addition, **11b** displayed a higher stability in human hepatocytes also compared to PQR626 ($t_{1/2}$: 164 min) [25]. The hepatocyte stability of **11b** was similar in the four species (human, rat, mouse, dog) tested allowing to use rats and dogs as toxicity assessment species, in contrast to PQR620 for which hepatocyte stability was much lower in humans compared to rats or dogs.

To characterize the CYP1A-related metabolism, compound **11b** was incubated with human CYP1A1 and CYP1A2. The CYP1A1 isoform is known to be involved in the degradation of chemically related triazine derivatives [44,47]. Stability towards CYP1A1 metabolism is considered an advantage in lead optimization programs as the high interindividual expression of CYP1A1 could lead to pharmacokinetic interindividual variability hampering the definition of a therapeutic dose. **11b** displayed a good to excellent stability after 60 min of incubation with CYP1A1 and CYP1A2, as indicated by 53.3% and 84.2% remaining compound, respectively (Fig. 5D).

3.6. Pharmacokinetics and plasma to brain partitioning after oral gavage

To assess the *in vivo* oral bioavailability, we investigate the pharmacokinetic profile of **11b** in male Sprague Dawley (SD) rats. After oral administration of a single dose of **11b** (5 mg/kg in 20% sulfobutyl-ether-β-cyclodextrins - SBECD, Captisol, Dexolve; Fig. 6A), its concentration in plasma and brain was determined. After 30 min, the maximal concentration (C_{max}) of **11b** was reached both in plasma and in the brain. A total exposure (AUC_{0-8}) of 3764 ng h/mL was reached in plasma after 8 h, while 2659 ng h/g was the AUC_{0-8} in brain. Thus, **11b** showed an excellent bioavailability after oral administration and good brain penetration with a brain:plasma distribution of 0.7:1 (see Fig. 6B).

We have previously disclosed potent pan-PI3K inhibitors, namely PQR309 [44], PQR514 [47], and PQR530 [49], that induced a fast rise of insulin and glucose plasma levels. Indeed, PI3Kα inhibitors are known to cause hyperglycaemia and hyperinsulinemia which are considered reliable markers for on-target activity [58]. On the contrary, **11b** did not

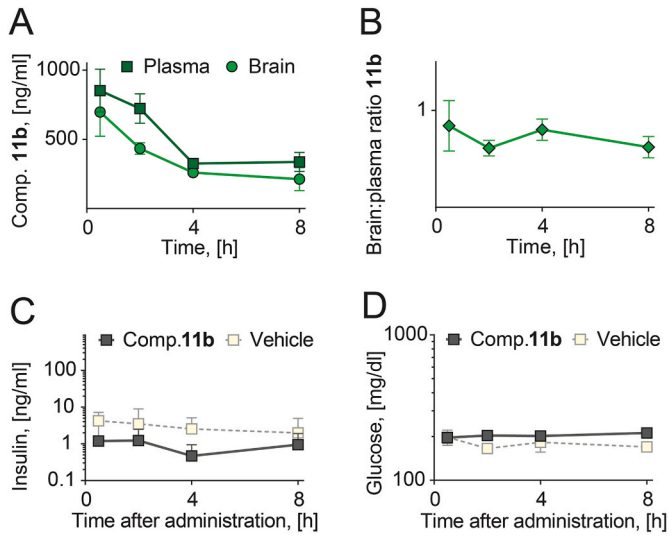

Fig. 6. PK and PD in male SD rats. (A) Concentration of compound **11b** in plasma and brain after p.o. administration (dose: 5 mg/kg). (B) Ratio of brain-to-plasma concentration over 8 h extracted from data shown in panel (A). (C, D) Plasma levels of insulin (C) and glucose (D) after oral dosing of **11b**. Experiments were performed in triplicate and data are shown as mean ± SD. Error bars are not depicted if smaller than the symbols. Raw data are summarized in Supporting Information (Tables S14–S19).

increase insulin and glucose concentrations when compared to the vehicle (Fig. 6C and D). These results highlight the ability of **11b** to selectively target mTOR.

3.7. Activity in lymphoma models

Aberrant activation of the PI3K/Akt/mTOR pathway is a hallmark of many cancers, including hematological malignancies [59,60], providing a rationale for the use of TORKi in the treatment of lymphomas. Thus, a subset of lymphoma cell lines previously exploited to assess the anti-proliferative activity of PQR620 [37] was selected. The anti-proliferative activity of the novel THP-derivative **11b** was investigated in three cell lines (VL51, SSK41 and KARPAS1718) derived from marginal zone lymphomas (MZL), a subset of lymphoma in which everolimus had also been clinically investigated [61]. As reference compounds everolimus and PQR620 were used, which have already been reported to be active in lymphoma [37,62], and **11a** (Fig. 7). Compounds **11b** and **11a** showed similar anti-proliferative activity in three cell lines (VL51: **11a** = 150.1, **11b** = 311 nM; SSK41: **11a** = 195.2, **11b** = 368.8 nM; KARPAS1718: **11a** = 353.5, **11b** = 117.8 nM). IC_{50}s values for **11b** and **11a** were similar to those observed with PQR620, while everolimus was – as expected – more potent (IC_{50}s < 0.001 nM).

Based on our previous data with both PQR309 and PQR620 [37,62], compounds **11a** and **11b** were combined with the BCL2 inhibitor venetoclax across a large range of concentrations to evaluate possible synergistic activity when concomitantly administered *in vitro*. Venetoclax is currently approved to treat patients with haematological malignancies, including chronic lymphocytic leukemia, small lymphocytic lymphoma, or acute myeloid leukemia [63], and has clinical activity against other lymphoma subtypes including MZL [64]. Based on the median Chou-Talalay Combination index values, the combination of **11b** with venetoclax was beneficial in all the three cell lines (synergism was observed in two, additivity in one; Table 6). Compound **11a** plus venetoclax achieved synergism in two of the three cell lines.

4. Conclusions

In summary, we have established a unique chemical space for ATP-competitive mTOR inhibitors, and investigated the effect of DHP and THP as isosters of the morpholine moiety. Molecular modelling elucidated the differential binding mode of DHP- and THP-substituted compounds, revealing the inability of the DHP and THP rings to form a strong hydrogen bond with the mTOR hinge region valine. The performed SAR study characterized **11b** as a potent and selective TORKi. Compound **11b** efficiently inhibited cellular mTOR signaling and showed a low turnover in CYP450 reactive phenotyping, which is an asset in drug discovery programs. In addition, **11b** showed excellent stability in human hepatocytes and good plasma and brain levels after p.o. administration. Compound **11b**, as well as **11a**, showed a dose-dependent anti-proliferative activity at sub-micromolar concentrations in lymphoma cell lines, which matched results obtained with PQR620 under the same settings and is comparable to previous work in other cell types [37].

The metabolic stability and the BBB permeability encourage the potential application of **11b** in the treatment of brain tumors, including lymphoma with primary or secondary CNS involvement, and chronic,

Table 6
Determination of synergy Combination Indexes (C.I.) for 11a/11b and/or of venetoclax.

	Median C.I.	95% range
11b-VL51	0.27	0.11–0.48
11b-SSK41	0.2	0.09–0.34
11b-KARPAS1718	0.91	0.51–1.66
11a-VL51	0.38	0.15–0.67
11a-SSK41	0.44	0.31–0.52
11a-KARPAS1718	2.53	1.55–3.6

Listed cell lines were exposed to selected compounds for 72 h. The combination effect was considered as beneficial if synergistic (<0.9) or additive (0-9-1.1), using the Chou-Talalay Combination Index. Values higher than 1.1 are suggestive of antagonism or no benefit.

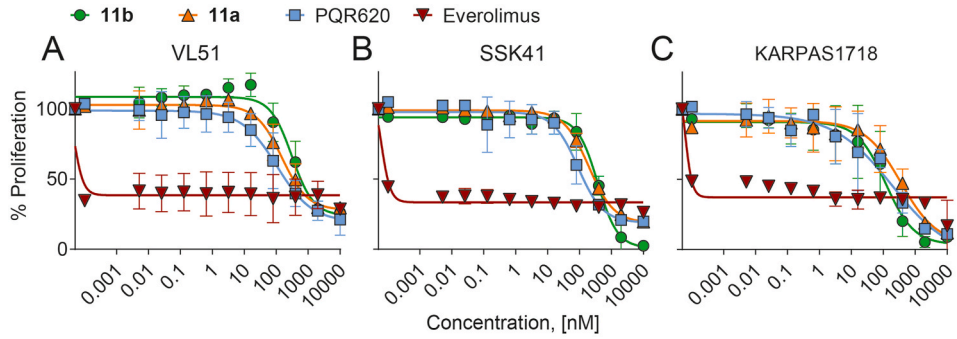

Fig. 7. Anti-proliferative activity of **11a**, **11b**, PQR620 and everolimus in splenic marginal zone lymphoma (SMZL) cell lines. Three SMZL cell lines (VL51, SSK41 and KARPAS1718) were exposed to increasing concentrations of **11a**, **11b**, PQR620, and everolimus, for 72 h.

neurological diseases, including epilepsy and Tuberous Sclerosis Complex.

Here, we show that DHP or preferentially THP substitution can replace a morpholine group bioisosterically in the solvent exposed region of the mTOR kinase binding site, but cannot functionally engage the Val2240 backbone nitrogen in the hinge region. In the case of **11b**, this results in a compound with an mTOR kinase selectivity comparable to PQR620, but with a significantly reduced lipophilicity. The latter is very likely responsible for the better metabolic stability in hepatocytes. Considering its mTOR potency/selectivity, CYP profile, its excellent stability in human hepatocytes, its suitable pharmacokinetic profile, and its anti-tumor as single agent and in combination with BCL2 inhibition, compound **11b** classifies as a novel TORKi to be further investigated in oncology.

5. Material and Methods

5.1. General experimental procedures

Reagents were purchased at the highest commercial quality from Acros, Sigma-Aldrich or Fluorochem and used without further purification. Solvents were purchased from Acros Organics in AcroSeal® bottles over molecular sieves. Cross coupling reactions were carried out under nitrogen atmosphere in anhydrous solvents, and glassware was oven dried prior to use. Thin layer chromatography (TLC) plates were purchased from Merck KGaA (Polygram SIL/UV254, 0.2 mm silica with fluorescence indicator) and UV light (254 nm) was used to visualize the compounds. Column chromatographic purifications were performed on Merck KGaA silica gel (pore size 60 Å, 230–400 mesh particle size). Alternatively, flash chromatography was performed with Isco Combi-Flash Companion systems using prepacked silica gel columns (40–60 μm particle size RediSep). 1H, 19F and 13C NMR spectra were recorded on a Bruker Avance 400 spectrometer. NMR spectra were obtained in deuterated solvents, such as $CDCl_3$, DMSO-d_6; in case of solubility issue, a mixture of $CDCl_3$ and CH_3OD was used for ^{13}C NMR. The chemical shift (δ values) are reported in ppm and corrected to the signal of the deuterated solvents (7.26 ppm (^1H NMR) and 77.16 ppm (^{13}C NMR) for $CDCl_3$; 2.50 ppm (^1H NMR) and 39.52 ppm (^{13}C NMR) for DMSO-d_6; and 3.31 ppm (^1H NMR) and 49.00 ppm (^{13}C NMR) for CD_3OD). ^{19}F NMR spectra are calibrated relative to $CFCl_3$ ($\delta = 0$ ppm) as external standard. When peak multiplicities are reported, the following abbreviations are used: s (singlet), d (doublet), dd (doublet of doublets), t (triplet), td (triplet of doublets), q (quartet), m (multiplet), br (broadened). Coupling constants, when given, are reported in Hertz (Hz). High resolution mass spectra (HRMS) were recorded on a Bruker maxis 4G, high resolution ESI-QTOF. All analysis were carried out in positive ion mode and in MeOH +0.1% formic acid as solvent. Sodium formate was used as calibration standard. MALDI-ToF mass spectra were obtained on a Voyager-De Pro measured in *m/z*. MS mass spectra, measured in *m/z*, were obtained on Thermo Scientific ISQ EC Single Quadrupole Mass Spectrometer integrated with high performance liquid chromatography (HPLC). High resolution mass spectra (HRMS) were recorded on a Bruker maxis 4G, high resolution ESI-QTOF. The chromatographic purity of final compounds was determined by high performance liquid chromatography (HPLC) analyses on an Ultimate 3000SD System from ThermoFisher with LPG-3400SD pump system, ACC-3000 autosampler and column oven, and DAD-3000 diode array detector. An Acclaim-120C18 reversed-phase column from ThermoFisher was used as stationary phase. Gradient elution (5:95 for 0.2 min, 5:95 → 100:0 over 10 min, 100:0 for 3 min) of the mobile phase consisting of CH_3CN/MeOH: $H_2O_{(10:90)}$ was used at a flow rate of 0.5 mL/min at 40 °C. The purity of all final compounds was >95%.

5.2. General procedures for the synthesis of the compounds

5.2.1. General procedure 1

Under nitrogen atmosphere, 3,6-dihydro-2*H*-pyran-4-boronic acid pinacol ester (1.1 eq.) was charged in a flask and dissolved in dioxane (approx. 1 mL/0.2 mmol). The respective di-chlorotriazine derivative (**12**–**17**, 1.0 eq.), K_3PO_4 (2 eq.) and [1,1′-bis(diphenylphosphino)ferrocene]dichloropalladium(II) [Pd(dppf)Cl_2, 0.05 eq.] and degassed, distilled H_2O:dioxane 1:6 were added. The reaction mixture was placed in a preheated oil bath at 85 °C and stirred at this temperature for 5 h. After completion of the reaction monitored by TLC, the mixture was diluted with deionized H_2O and the aqueous layer was extracted with EtOAc (3x). The combined organic layers were dried over anhydrous Na_2SO_4, filtered and reduced to dryness under reduced pressure. The crude product was purified by column chromatography on silica gel.

5.2.2. General procedure 2

Under nitrogen atmosphere, the respective boronic ester (**24**, **25**, **28**, 1.1–1.5 eq.) was charged in a flask and dissolved in dioxane (approx. 1 mL/0.16 mmol). The respective mono-chlorotriazine derivative (**18–23**, 1.0 eq.), K_3PO_4 (2 eq.) and chloro(2-dicyclohexylphosphino-2′,4′,6′-triisopropyl-1,1′-biphenyl)[2-(2′-amino-1,1′-biphenyl)]-palladium(II) (XPhosPdG2, 0.05 eq.) and degassed distilled H2O:dioxane 1:6 were added. The reaction mixture was placed in a preheated oil bath at 95 °C and stirred at this temperature for 3–6 h. After completion of the reaction monitored by TLC, a 3 M aqueous HCl-solution (10 eq.) was added and the mixture was stirred at 80 °C for 3 h. After completion of the reaction monitored by TLC, reaction was allowed to cool down and a 2 M aqueous NaOH-solution was added until pH 9–10. The aqueous layer was extracted with EtOAc (3x). The combined organic layers were dried over anhydrous Na_2SO_4, filtered and the solvent was evaporated under reduced pressure. The crude product was purified by column chromatography on silica gel.

5.2.3. General procedure 3

Step 1. Bis(pinacolato)diboron (1.5 eq.), potassium acetate (3.0 eq.), [1,1′-bis(diphenylphosphino)ferrocene]dichloropalladium(II) (Pd(dppf)Cl_2, 0.10 eq.) and the respective bromo derivative (**26**, **27**, 1.0 eq.) were dissolved in 1,4-dioxane (approx. 1 mL/0.1 mmol) under nitrogen atmosphere. The resulting mixture was heated at 95 °C for 2–4 h.

Step 2. Then, the mixture was allowed to cool down to room temperature. Mono-chlorotriazine derivative precursor (**18**, 1.0 eq.), chloro(2-dicyclohexylphosphino-2′,4′,6′-triisopropyl-1,1′-biphenyl)[2-(2′-amino-1,1′-biphenyl)]palladium(II) (XPhosPdG2, 0.05 eq.), potassium phosphate (3.0 eq.), and deionized H_2O (approx. 1 mL/0.3 mmol) were added. The resulting reaction mixture was placed in a preheated oil bath at 95 °C and stirred for 2–15 h.

Step 3. After completion of the reaction, the mixture was allowed to cool down to room temperature and an aq. solution of HCl (3 M, 10–20 eq.) was added. The reaction mixture was stirred at 80 °C for 3 h. The mixture was diluted with deionized H_2O and washed with EtOAc (1x). The aq. layer was basified to pH = 10–11 and then extracted with EtOAc (3x). The combined organic layers were dried over anhydrous Na_2SO_4, filtered and reduced to dryness under reduced pressure. The crude product was purified by column chromatography on silica gel.

5.2.4. General procedure 4

Under nitrogen atmosphere, the respective saturated compound **1a-11a** (1.0 eq.) was charged in a flask and dissolved in MeOH (approx. 1 ml/0.15 mmol), Pd/C (10%) was added. Nitrogen was removed and the reaction flask was filled with hydrogen. The reaction mixture was stirred at 25–40 °C for 24–72 h. After completion of the reaction monitored by TLC, the solvent was evaporated under reduced pressure. DCM was

added (10 mL) and the mixture was filtered through a pad of Celite and concentrated in vacuum. The crude product was purified by column chromatography on silica gel.

5.3. Synthesis of compounds

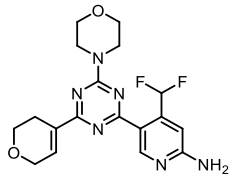

4-(difluoromethyl)-5-(4-(3,6-dihydro-2*H*-pyran-4-yl)-6-morpholino-1,3,5-triazin-2-yl)pyridin-2-amine (1a) was prepared according to general procedure 2 from intermediate **18** (300 mg, 1.06 mmol, 1.0 eq.) and *N*'-[4-(difluoromethyl)-5-(4,4,5,5-tetramethyl-1,3,2-dioxaborolan-2-yl)pyridin-2-yl]-*N*,*N*-dimethylmethanimidamide **24** (380 mg, 1.17 mmol, 1.1 eq.). Purification by column chromatography on silica gel (cyclohexane/ethyl acetate 1:0 → 3:7) gave compound **1a** as a colourless solid (186 mg, 0.48 mmol, 45%). **^{1}H NMR** (400 MHz, DMSO-d_6): δ 8.99 (s, 1H), 7.82 (t, J = 55.1 Hz, 1H), 7.36 (s, 1H), 6.99 (s, 2H), 6.80 (s, 1H), 4.33–4.31 (m, 2H), 3.87–3.84 (m, 4H), 3.82–3.79 (m, 2H), 3.70–3.69 (m, 4H). **^{19}F{^{1}H} NMR** (376 MHz, DMSO-d_6): δ −116.10 (s, 2F). **^{13}C{^{1}H} NMR (**101 MHz, DMSO-d_6): δ 169.94 (s, 1C), 169.62 (s, 1C), 164.46 (s, 1C), 162.26 (s, 1C), 153.05 (s, 1C), 142.79 (d, J = 21.6 Hz, 1C), 134.89 (s, 1C), 133.24 (s, 1C), 117.82 (s, 1C), 112.24 (t, J = 237.5 Hz, 1C), 103.86 (t, J = 8.4 Hz, 1C), 66.35 (s, 2C), 65.56 (s, 1C), 63.97 (s, 1C), 43.76 (s, 2C), 24.94 (s, 1C). **HRMS** (*m/z*): [M + H]$^+$ calc. for $C_{18}H_{21}F_2N_6O_2$ 391.1689; found: 391.1690. **HPLC** (ACN with 0.1% TFA): t_R = 6.27 min (96.25% purity).

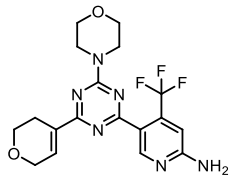

5-(4-(3,6-dihydro-2*H*-pyran-4-yl)-6-morpholino-1,3,5-triazin-2-yl)-4-(trifluoromethyl)pyridin-2-amine (2a) was prepared according to general procedure 2 from intermediate **18** (150 mg, 0.53 mmol, 1.0 eq.) and (*E*)-*N*,*N*-dimethyl-*N*'-(5-(4,4,5,5-tetramethyl-1,3,2-dioxaborolan-2-yl)-4-(trifluoromethyl)pyridin-2-yl)formimidamide **25** (236 mg, 0.69 mmol, 1.3 eq.). Purification by column chromatography on silica gel (cyclohexane/ethyl acetate 1:0 → 0:1) gave compound **2a** as a colourless solid (112 mg, 0.28 mmol, 52%). **^{1}H NMR** (400 MHz, $CDCl_3$): δ 8.81 (s, 1H), 7.40 (dt, J = 3.0, 1.4 Hz, 1H), 6.82 (s, 1H), 4.92 (s, 2H), 4.40 (q, J = 2.8 Hz, 2H), 3.99–3.87 (m, 6H), 3.78–3.76 (m, 4H), 2.68–2.62 (m, 2H). **^{19}F{^{1}H} NMR** (376 MHz, $CDCl_3$): δ −60.12 (s, 3F). **^{13}C{^{1}H} NMR (**101 MHz, DMSO-d_6): δ 170.41 (s, 1C), 169.95 (s, 1C), 164.37 (s, 1C), 160.02 (s, 1C), 152.70 (s, 1C), 138.60 (q, J = 32.9 Hz, 1C), 133.94 (s, 1C), 133.51 (s, 1C), 122.75 (q, J = 274.4 Hz, 1C), 121.06–121.00 (m, 1C), 106.08–105.52 (m, 1C), 66.70 (s, 2C), 65.83 (s, 1C), 64.42 (s, 1C), 43.57 (s, 2C), 24.78 (s, 1C). **HRMS** (*m/z*): [M + H]$^+$ calc. for $C_{18}H_{20}F_3N_6O_2$ 409.1594; found: 409.1602. **HPLC** (ACN with 0.1% TFA): t_R = 6.93 min (97.65% purity).

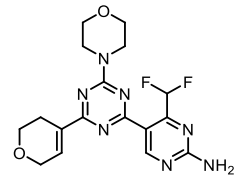

4-(difluoromethyl)-5-(4-(3,6-dihydro-2*H*-pyran-4-yl)-6-morpholino-1,3,5-triazin-2-yl)pyrimidin-2-amine (3a) was prepared according to general procedure 3 from intermediate **18** (200 mg, 0.70 mmol, 1.1 eq.) and *tert*-butyl (5-bromo-4-(difluoromethyl)pyrimidin-2-yl)(*tert*-butoxycarbonyl)carbamate **26** (272 mg, 0.64 mmol, 1.0 eq.). Purification by column chromatography on silica gel (cyclohexane/ethyl acetate 1:0 → 3:7) gave compound **3a** as a colourless solid (178 mg, 0.46 mmol, 65%). **^{1}H NMR** (400 MHz, DMSO-d_6): δ 9.20 (s, 1H), 7.82–7.55 (m, 2H), 7.68 (t, J = 53.9 Hz, 1H), 7.40–7.36 (m, 1H), 4.33 (m, 2H), 3.87 (m, 5H), 3.81 (t, J = 5.4 Hz, 2H), 3.69 (m, 5H). **^{19}F{^{1}H} NMR** (376 MHz, DMSO-d_6): δ −120.91 (s, 2F). **^{13}C{^{1}H} NMR (**101 MHz, DMSO-d_6): δ 170.09 (s, 1C), 168.19 (s, 1C), 164.42 (s, 1C), 164.18 (s, 1C), 162.43 (s, 1C), 159.91 (s, 1C), 135.33 (s, 1C), 133.10 (s, 1C), 117.32 (t, J = 3.5 Hz, 1C), 110.37 (t, J = 239.4 Hz, 1C), 66.33 (s, 2C), 65.56 (s, 1C), 63.94 (s, 1C), 43.80 (br s, 2C), 24.89 (s, 1C). **HRMS** (*m/z*): [M + H]$^+$ calc. for $C_{17}H_{20}F_2N_7O_2$ 392.1641; found: 392.1648. **HPLC** (ACN with 0.1% TFA): t_R = 5.44 min (>99% purity).

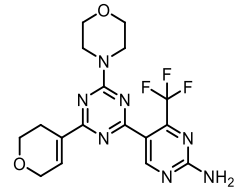

5-(4-(3,6-dihydro-2*H*-pyran-4-yl)-6-morpholino-1,3,5-triazin-2-yl)-4-(trifluoromethyl)pyrimidin-2-amine (4a) was prepared according to general procedure 3 from intermediate **18** (280 mg, 0.99 mmol, 1.0 eq.) and *tert*-butyl (5-bromo-4-(trifluoromethyl)pyrimidin-2-yl)(*tert*-butoxycarbonyl)carbamate **27** (400 mg, 1.35 mmol, 1.3 eq.). Purification by column chromatography on silica gel (cyclohexane/ethyl acetate 1:0 → 0:1) gave compound **4a** as a colourless solid (157 mg, 0.38 mmol, 39%). **^{1}H NMR** (400 MHz, DMSO-d_6): δ 8.99 (s, 1H), 7.80 (s, 2H), 7.40–7.36 (m, 1H), 4.35–4.29 (m, 2H), 3.90–3.82 (m, 5H), 3.79 (t, J = 5.4 Hz, 2H), 3.72–3.64 (t, J = 4.7 Hz, 5H). **^{19}F{^{1}H} NMR** (376 MHz, DMSO-d_6): δ −64.22 (s, 3F). **^{13}C{^{1}H} NMR (**101 MHz, DMSO-d_6): 170.25 (s, 1C), 168.82 (s, 1C), 164.22 (s, 1C), 163.72 (s, 1C), 163.47 (s, 1C), 153.70 (q, J = 34.6 Hz, 1C), 135.46 (s, 1C), 133.06 (s, 1C), 121.19 (q, J = 276.2 Hz, 1C), 117.87 (s, 1C), 66.31 (s, 2C), 65.54 (s, 1C), 63.92 (s, 1C), 43.74 (s, 2C), 24.87 (s, 1C). **HRMS** (*m/z*): [M + H]$^+$ calc. for $C_{17}H_{19}F_3N_7O_2$ 410.1547; found: 410.1552. **HPLC** (ACN with 0.1% TFA): t_R = 7.85 min (97.84% purity).

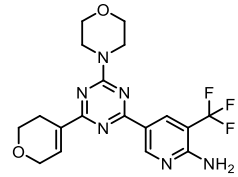

5-(4-(3,6-dihydro-2*H*-pyran-4-yl)-6-morpholino-1,3,5-triazin-2-yl)-3-(trifluoromethyl)pyridin-2-amine (5a) was prepared according to general procedure 2 from intermediate **18** (273 mg, 0.97 mmol, 1.0 eq.) and (*E*)-*N*,*N*-dimethyl-*N*'-(5-(4,4,5,5-tetramethyl-1,3,2-dioxaborolan-2-yl)-3-(trifluoromethyl)pyridin-2-yl)formimidamide **28** (398 mg, 1.16 mmol, 1.2 eq.). Purification by column chromatography on silica

gel (cyclohexane/ethyl acetate 1:0 → 0:1) gave compound **5a** as a colourless solid (138 mg, 0.34 mmol, 35%). **^{1}H NMR** (400 MHz, $CDCl_3$): δ 9.29 (br s, 1H), 8.72 (br s, 1H), 7.45–7.40 (m, 1H), 5.30 (s, 2H), 4.43–4.41 (m, 2H), 4.02–3.94 (m, 4H), 3.92 (t, J = 5.4 Hz, 2H), 3.83–3.77 (m, 4H), 2.71–2.64 (m, 2H). **^{19}F{^{1}H} NMR** (376 MHz, $CDCl_3$): δ −64.16 (s, 3F). **^{13}C{^{1}H} NMR** (101 MHz, $CDCl_3$): δ 170.52 (s, 1C), 168.20 (s, 1C), 164.60 (s, 1C), 156.85 (q, J = 1.5 Hz, 1C), 153.26 (m, 1C), 135.73 (q, J = 5.0 Hz, 1C), 133.87 (s, 1C), 133.71 (s, 1C), 124.14 (q, J = 271.6 Hz, 1C), 122.50 (s, 1C), 107.85 (q, J = 32.6 Hz, 1C), 66.77 (s, 2C), 65.88 (s, 1C), 64.45 (s, 1C), 43.63 (br s, 2C), 24.91 (s, 1C). **HRMS** (m/z): [M + H]$^+$ calc. for $C_{18}H_{20}F_3N_6O_2$ 409.1594; found: 409.1601. **HPLC**: t_R = 9.48 min (95.47% purity).

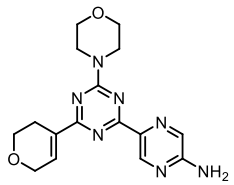

5-(4-(3,6-dihydro-2*H*-pyran-4-yl)-6-morpholino-1,3,5-triazin-2-yl)pyrazin-2-amine (6a). Under nitrogen atmosphere, 5-aminopyrazine-2-boronic acid (310 mg, 1.41 mmol, 1.1 eq.) was charged in a flask and dissolved in dioxane (approx. 1 mL/0.16 mmol). Intermediate **18** (360 mg, 1.28 mmol, 1.0 eq.), K_3PO_4 (2 eq.) and chloro(2-dicyclohexylphosphino-2′,4′,6′-triisopropyl-1,1′-biphenyl)[2-(2′-amino-1,1′-biphenyl)]-palladium(II) (XPhosPdG2, 0.05 eq.) and degassed distilled H_2O:dioxane 1:6 were added. The reaction mixture was placed in a preheated oil bath at 95 °C and stirred at this temperature for 4 h. After completion of the reaction monitored by TLC, the mixture was diluted with deionized H_2O. The aqueous layer was extracted with EtOAc (3x). The combined organic layers were dried over anhydrous Na_2SO_4, filtered and the solvent was evaporated under reduced pressure. Purification by column chromatography on silica gel (cyclohexane/ethyl acetate 1:0 → 0:1) gave compound **6a** as a colourless solid (141 mg, 0.41 mmol, 32%). **^{1}H NMR** (400 MHz, $CDCl_3$): δ 9.69 (d, J = 1.1 Hz, 1H), 8.29 (dd, J = 2.4, 1.6 Hz, 1H), 8.24 (d, J = 2.6 Hz, 1H), 8.16 (br s, 1H), 7.32–7.28 (m, 1H), 4.38 (q, J = 2.7 Hz, 2H), 3.97–3.82 (m, 6H), 3.80–3.70 (m, 4H), 2.64–2.58 (m, 2H). **^{13}C{^{1}H} NMR** (101 MHz, $CDCl_3$): δ 171.06 (s, 1C), 164.86 (s, 1C), 163.49 (s, 1C), 149.27 (s, 1C), 142.13 (s, 1C), 138.19 (s, 1C), 137.01 (s, 1C), 133.64 (s, 1C), 133.49 (s, 1C), 66.70 (s, 2C), 65.81 (s, 1C), 64.41 (s, 1C), 43.80 (s, 2C), 25.00 (s, 1C). **HRMS** (m/z): [M + H]$^+$ calc. for $C_{16}H_{20}N_7O_2$ 342.1673; found: 342.1679. **HPLC**: t_R = 7.08 min (97.13% purity).

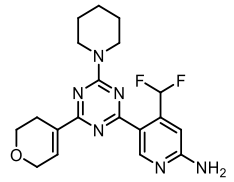

4-(difluoromethyl)-5-(4-(3,6-dihydro-2*H*-pyran-4-yl)-6-(piperidin-1-yl)-1,3,5-triazin-2-yl)pyridin-2-amine (7a) was prepared according to general procedure 2 from intermediate **19** (130 mg, 0.46 mmol, 1.0 eq.) and *N*'-[4-(difluoromethyl)-5-(4,4,5,5-tetramethyl-1,3,2-dioxaborolan-2-yl)pyridin-2-yl]-*N*,*N*-dimethylmethanimidamide **24** (181 mg, 0.55 mmol, 1.2 eq.). Purification by column chromatography on silica gel (cyclohexane/ethyl acetate 1:0 → 3:7) gave compound **7a** as a colourless solid (89 mg, 0.23 mmol, 50%). **^{1}H NMR** (400 MHz, $CDCl_3$): δ 8.97 (s, 1H), 7.70 (t, J = 55.2 Hz, 1H), 7.26 (s, 1H), 6.81 (s, 1H), 4.37–4.32 (m, 2H), 3.90–3.76 (m, 6H), 3.12 (s, 2H), 2.62–2.55 (m, 2H), 1.70–1.53 (m, 6H). **^{19}F{^{1}H} NMR** (376 MHz, $CDCl_3$): δ −116.79 (s, 2F). **^{13}C{^{1}H} NMR** (101 MHz, $CDCl_3$): δ 170.07 (s, 1C), 169.22 (s, 1C), 163.92 (s, 1C), 160.45 (s, 1C), 151.94 (s, 1C), 143.95 (t, J = 22.1 Hz, 1C), 133.75 (s, 1C), 133.08 (s, 1C), 120.49 (t, J = 4.7 Hz, 1C), 111.26 (t, J = 238.9 Hz, 1C), 104.56 (t, J = 8.3 Hz, 1C), 65.81 (s, 1C), 64.46 (s, 1C), 44.31 (s, 2C), 25.70 (s, 2C), 24.82 (s, 1C), 24.63 (s, 1C). **HRMS** (m/z): [M + H]$^+$ calc. for $C_{19}H_{23}F_2N_6O$ 389.1896; found: 389.1902. **HPLC**: t_R = 9.56 min (97.42% purity).

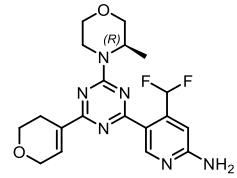

(*R*)-4-(difluoromethyl)-5-(4-(3,6-dihydro-2*H*-pyran-4-yl)-6-(3-methylmorpholino)-1,3,5-triazin-2-yl)pyridin-2-amine (8a) was prepared according to general procedure 2 from intermediate **20** (200 mg, 0.67 mmol, 1.0 eq.) and *N*'-[4-(difluoromethyl)-5-(4,4,5,5-tetramethyl-1,3,2-dioxaborolan-2-yl)pyridin-2-yl]-*N*,*N*-dimethylmethanimidamide **24** (328 mg, 1.01 mmol, 1.5 eq.). Purification by column chromatography on silica gel (cyclohexane/ethyl acetate 1:0 → 3:7) gave compound **8a** as a colourless solid (60.5 mg, 0.15 mmol, 22%). **^{1}H NMR** (400 MHz, $CDCl_3$): δ 9.13 (s, 1H), 7.77 (t, J = 55.2 Hz, 1H), 7.38–7.34 (m, 1H), 6.85 (s, 1H), 5.05 (s, 2H), 4.83 (br s, 1H), 4.51 (br s, 1H), 4.40 (q, J = 2.8 Hz, 2H), 4.01 (dd, J = 11.5, 3.7 Hz, 1H), 3.90 (t, J = 5.5 Hz, 2H), 3.80 (d, J = 11.5 Hz, 1H), 3.70 (dd, J = 11.5, 3.3 Hz, 1H), 3.55 (td, J = 11.9, 2.9 Hz, 1H), 3.33 (t, J = 12.5 Hz, 1H), 2.68–2.58 (m, 2H), 1.35 (d, J = 7.0 Hz, 3H). **^{19}F{^{1}H} NMR** (376 MHz, $CDCl_3$): δ −116.29 (s, 2F). **^{13}C{^{1}H} NMR** (101 MHz, $CDCl_3$): δ 170.29 (s, 1C), 169.48 (s, 1C), 164.14 (s, 1C), 160.46 (s, 1C), 152.73 (s, 1C), 143.86 (t, J = 22.1 Hz, 1C), 133.86 (s, 1C), 133.68 (s, 1C), 120.63 (t, J = 4.7 Hz, 1C), 111.32 (t, J = 238.9 Hz, 1C), 104.20 (t, J = 8.3 Hz, 1C), 70.98 (s, 1C), 66.91 (s, 1C), 65.89 (s, 1C), 64.44 (s, 1C), 46.56 (s, 1C), 38.63 (s, 1C), 24.91 (s, 1C), 14.33 (s, 1C). **HRMS** (m/z): [M + H]$^+$ calc. for $C_{19}H_{23}F_2N_6O_2$ 405.1845; found: 405.1853. **HPLC**: t_R = 8.17 min (>99% purity).

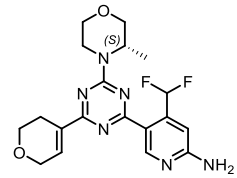

(*S*)-4-(difluoromethyl)-5-(4-(3,6-dihydro-2*H*-pyran-4-yl)-6-(3-methylmorpholino)-1,3,5-triazin-2-yl)pyridin-2-amine (9a) was prepared according to general procedure 2 from intermediate **21** (132 mg, 0.44 mmol, 1.0 eq.) and *N*'-[4-(difluoromethyl)-5-(4,4,5,5-tetramethyl-1,3,2-dioxaborolan-2-yl)pyridin-2-yl]-*N*,*N*-dimethylmethanimidamide **24** (174 mg, 0.53 mmol, 1.2 eq.). Purification by column chromatography on silica gel (cyclohexane/ethyl acetate 1:0 → 3:7) gave compound **9a** as a colourless solid (20.7 mg, 0.05 mmol, 12%). **^{1}H NMR** (400 MHz, $CDCl_3$): δ 9.13 (s, 1H), 7.77 (t, J = 55.2 Hz, 1H), 7.38–7.33 (m, 1H), 6.86 (s, 1H), 4.99 (s, 2H), 4.84 (br s, 1H), 4.52 (br s, 1H), 4.41 (q, J = 2.8 Hz, 2H), 4.01 (dd, J = 11.5, 3.8 Hz, 1H), 3.91 (t, J = 5.5 Hz, 2H), 3.80 (d, J = 11.5 Hz, 1H), 3.70 (dd, J = 11.5, 3.3 Hz, 1H), 3.55 (td, J = 11.9, 3.0 Hz, 1H), 3.33 (td, J = 13.2, 3.8 Hz, 1H), 2.68–2.60 (m, 2H), 1.36 (d, J = 6.9 Hz, 3H). **^{19}F{^{1}H} NMR** (376 MHz, $CDCl_3$): δ −116.81 (s, 2F). **^{13}C{^{1}H} NMR** (101 MHz, $CDCl_3$): δ 170.29 (s, 1C), 169.49 (s, 1C), 164.14 (s, 1C), 160.41 (s, 1C), 152.74 (s, 1C), 143.87 (t, J = 22.2 Hz, 1C), 133.87 (s, 1C), 133.68 (s, 1C), 120.68 (t, J = 4.7 Hz, 1C), 111.32 (t, J = 238.9 Hz, 1C), 104.18 (t, J = 8.3 Hz, 1C), 70.98 (s, 1C), 66.92 (s, 1C), 65.90 (s, 1C), 64.44 (s, 1C), 46.56 (s, 1C), 38.63 (s, 1C), 24.91 (s, 1C), 14.34 (s, 1C). **HRMS** (m/z): [M + H]$^+$ calc. for

$C_{19}H_{23}F_2N_6O_2$ 405.1845; found: 405.1848. **HPLC**: t_R = 8.21 min (98.16% purity).

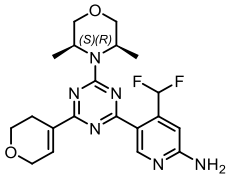

4-(difluoromethyl)-5-(4-(3,6-dihydro-2*H*-pyran-4-yl)-6-((3*R*,5*S*)-3,5-dimethylmorpholino)-1,3,5-triazin-2-yl)pyridin-2-amine (10a) was prepared according to general procedure 2 from intermediate **22** (355 mg, 1.14 mmol, 1.0 eq.) and *N'*-[4-(difluoromethyl)-5-(4,4,5,5-tetramethyl-1,3,2-dioxaborolan-2-yl)pyridin-2-yl]-*N*,*N*-dimethylmethanimidamide **24** (446 mg, 1.37 mmol, 1.1 eq.). Purification by column chromatography on silica gel (cyclohexane/ethyl acetate 1:0 → 3:7) gave compound **10a** as a colourless solid (152 mg, 0.36 mmol, 32%). **^{1}H NMR** (400 MHz, $CDCl_3$): δ 9.16 (s, 1H), 7.81 (t, J = 55.3 Hz, 1H), 7.38–7.34 (m, 1H), 6.86 (s, 1H), 5.01 (s, 2H), 4.71–4.62 (m, 2H), 4.41 (q, J = 2.8 Hz, 2H), 3.91 (t, J = 5.4 Hz, 2H), 3.86 (d, J = 11.6 Hz, 2H), 3.68 (dd, J = 11.6, 3.9 Hz, 2H), 2.68–2.61 (m, 2H), 1.40 (d, J = 6.9 Hz, 6H). **^{19}F{^{1}H} NMR** (376 MHz, $CDCl_3$): δ −116.29 (s, 2F). **^{13}C{^{1}H} NMR** (101 MHz, $CDCl_3$): δ 170.17 (s, 1C), 169.36 (s, 1C), 163.77 (s, 1C), 160.39 (s, 1C), 152.78 (s, 1C), 143.87 (t, J = 22.1 Hz, 1C), 133.77 (s, 1C), 133.65 (s, 1C), 120.75 (t, J = 4.7 Hz, 1C), 111.34 (t, J = 238.9 Hz, 1C), 104.15 (t, J = 8.3 Hz, 1C), 71.32 (s, 2C), 65.91 (s, 1C), 64.47 (s, 1C), 45.95 (s, 2C), 24.91 (s, 1C), 18.95 (s, 2C). **HRMS** (m/z): $[M + H]^+$ calc. for $C_{20}H_{25}F_2N_6O_2$ 419.2002; found: 419.200. **HPLC**: t_R = 9.30 min (99.47% purity).

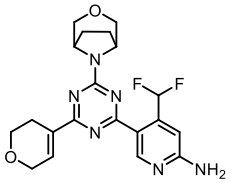

5-(4-(3-oxa-8-azabicyclo[3.2.1]octan-8-yl)-6-(3,6-dihydro-2*H*-pyran-4-yl)-1,3,5-triazin-2-yl)-4-(difluoromethyl)pyridin-2-amine (11a) was prepared according to general procedure 2 from intermediate **23** (250 mg, 0.80 mmol, 1.0 eq.) and *N'*-[4-(difluoromethyl)-5-(4,4,5,5-tetramethyl-1,3,2-dioxaborolan-2-yl)pyridin-2-yl]-*N*,*N*-dimethylmethanimidamide **24** (314 mg, 0.96 mmol, 1.2 eq.). Purification by column chromatography on silica gel (cyclohexane/ethyl acetate 1:0 → 3:7) gave compound **11a** as a colourless solid (116 mg, 0.28 mmol, 35%). **^{1}H NMR** (400 MHz, DMSO-d_6): δ 8.99 (s, 1H), 7.82 (t, J = 55.1 Hz, 1H), 7.36–7.32 (m, 1H), 7.00–6.95 (m, 2H), 6.80 (s, 1H), 4.76–4.70 (m, 2H), 4.34–4.30 (m, 2H), 3.80 (t, J = 5.5 Hz, 2H), 3.69–3.57 (m, 4H), 2.56–2.52 (m, 2H), 2.06–1.92 (m, 4H). **^{19}F{^{1}H} NMR** (376 MHz, DMSO-d_6): δ −116.00 (s, 2F). **^{13}C{^{1}H} NMR** (101 MHz, DMSO-d_6): δ 169.76 (s, 1C), 169.41 (s, 1C), 161.99 (s, 1C), 161.93 (s, 1C), 152.59 (s, 1C), 142.45 (t, J = 21.7 Hz, 1C), 134.29 (s, 1C), 132.78 (s, 1C), 117.31 (t, J = 4.6 Hz, 1C), 111.81 (t, J = 236.1 Hz, 1C), 103.40 (t, J = 8.4 Hz, 1C), 70.95 (s, 1C), 70.90 (s, 1C), 65.08 (s, 1C), 63.50 (s, 1C), 54.51 (s, 1C), 54.43 (s, 1C), 26.40 (s, 1C), 26.33 (s, 1C), 24.46 (s, 1C). **HRMS** (m/z): $[M + H]^+$ calc. for $C_{20}H_{23}F_2N_6O_2$ 417.1845; found: 417.1851. **HPLC**: t_R = 8.19 min (96.98% purity).

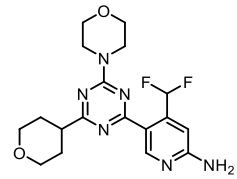

4-(difluoromethyl)-5-(4-morpholino-6-(tetrahydro-2*H*-pyran-4-yl)-1,3,5-triazin-2-yl)pyridin-2-amine (1b) was prepared according to general procedure 4 from **1a** (164 mg, 0.42 mmol, 1.0 eq.). Purification by column chromatography on silica gel (cyclohexane/ethyl acetate 1:0 → 0:1) gave compound **1b** as a colourless solid (71.3 mg, 0.18 mmol, 43%). **^{1}H NMR** (400 MHz, $CDCl_3$): δ 9.10 (s, 1H), 7.80 (t, J = 55.3 Hz, 1H), 6.85 (s, 1H), 4.92 (s, 2H), 4.07 (dt, J = 11.3, 3.4 Hz, 2H), 3.96–3.89 (m, 4H), 3.81–3.75 (m, 4H), 3.58–3.50 (m, 2H), 2.90–2.80 (m, 1H), 1.98–1.91 (m, 4H). **^{19}F{^{1}H} NMR** (376 MHz, CDCl3): δ −117.37 (s, 2F). **^{13}C{^{1}H} NMR** (101 MHz, $CDCl_3$): δ 178.22 (s, 1C), 168.06 (s, 1C), 162.61 (s, 1C), 159.11 (s, 1C), 150.42 (s, 1C), 142.41 (t, J = 22.1 Hz, 1C), 118.08 (t, J = 4.5 Hz, 1C), 109.59 (t, J = 239.0 Hz, 1C), 103.10 (t, J = 8.7 Hz, 1C), 66.05 (s, 2C), 65.01 (s, 2C), 41.90 (s, 2C), 41.85 (s, 1C), 28.76 (s, 2C). **HRMS** (m/z): $[M + H]^+$ calc. for $C_{18}H_{23}F_2N_6O_2$ 393.1845; found: 393.1852. **HPLC**: t_R = 7.37 min (95.05% purity).

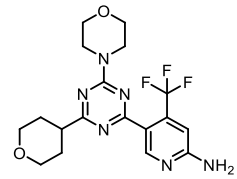

5-(4-morpholino-6-(tetrahydro-2*H*-pyran-4-yl)-1,3,5-triazin-2-yl)-4-(trifluoromethyl)pyridin-2-amine (2b) was prepared according to general procedure 4 from **2a** (143 mg, 0.35 mmol, 1.0 eq.). Purification by column chromatography on silica gel (cyclohexane/ethyl acetate 1:0 → 0:1) gave compound **2b** as a colourless solid (32.4 mg, 0.08 mmol, 23%). **^{1}H NMR** (400 MHz, $CDCl_3$): δ 8.76 (s, 1H), 6.81 (s, 1H), 4.92 (s, 2H), 4.06 (dt, J = 11.5, 3.6 Hz, 2H), 3.92 (br s, 4H), 3.80–3.72 (m, 4H), 3.58–3.49 (m, 2H), 2.87 (tt, J = 10.2, 5.4 Hz, 1H), 2.05–1.91 (m, 4H). **^{19}F{^{1}H} NMR** (376 MHz, CDCl3): δ −60.10 (s, 3F). **^{13}C{^{1}H} NMR** (101 MHz, $CDCl_3$): δ 180.07 (s, 1C), 170.22 (s, 1C), 164.23 (s, 1C), 160.10 (s, 1C), 152.51 (s, 1C), 138.62 (q, J = 32.8 Hz, 1C), 122.77 (q, J = 274.1 Hz, 1C), 120.84–120.78 (m, 1C), 106.12–105.91 (m, 1C), 67.72 (s, 2C), 66.70 (s, 2C), 43.56 (s, 2C), 43.52 (s, 1C), 30.41 (s, 2C). **HRMS** (m/z): $[M + H]^+$ calc. for $C_{18}H_{22}F_3N_6O_2$ 411.1751; found: 411.1756. **HPLC** (ACN with 0.1% TFA): t_R = 6.47 min (96.63% purity).

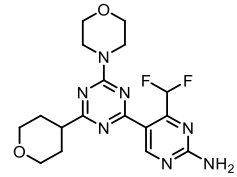

4-(difluoromethyl)-5-(4-morpholino-6-(tetrahydro-2*H*-pyran-4-yl)-1,3,5-triazin-2-yl)pyrimidin-2-amine (3b) was prepared according to general procedure 4 from **3a** (137 mg, 0.35 mmol, 1.0 eq.). Purification by column chromatography on silica gel (cyclohexane/ethyl acetate 1:0 → 0:1) gave compound **3b** as a colourless solid (48.2 mg, 0.13 mmol, 35%). **^{1}H NMR** (400 MHz, $CDCl_3$): δ 9.30 (s, 1H), 7.74 (t, J = 54.3 Hz, 1H), 6.11 (s, 2H), 4.07 (dt, J = 11.3, 3.4 Hz, 2H), 3.98–3.87 (m, 4H), 3.82–3.73 (m, 4H), 3.58–3.49 (m, 2H), 2.91–2.80 (m, 1H), 1.98–1.89 (m, 4H). **^{19}F{^{1}H} NMR** (376 MHz, CDCl3): δ −122.37 (s, 2F).

^{13}C{^{1}H} NMR (101 MHz, $CDCl_3$): δ 180.34 (s, 1C), 168.05 (s, 1C), 164.19 (s, 1C), 163.28 (s, 1C), 162.30 (s, 1C), 160.41 (t, J = 21.5 Hz, 1C), 118.88 (t, J = 3.4 Hz, 1C), 109.47 (t, J = 241.3 Hz, 1C), 67.65 (s, 2C), 66.63 (s, 2C), 43.65 (s, 3C), 30.47 (s, 2C). **HRMS** (m/z): $[M + H]^+$ calc. for $C_{17}H_{22}F_2N_7O_2$ 394.1798; found: 394.1803. **HPLC** (ACN with 0.1% TFA): t_R = 6.90 min (97.34% purity).

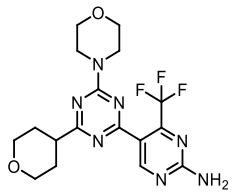

5-(4-morpholino-6-(tetrahydro-2*H*-pyran-4-yl)-1,3,5-triazin-2-yl)-4-(trifluoromethyl)pyrimidin-2-amine (4b) was prepared according to general procedure 4 from **4a** (150 mg, 0.37 mmol, 1.0 eq.). Purification by column chromatography on silica gel (cyclohexane/ethyl acetate 1:0 → 0:1) gave compound **4b** as a colourless solid (48.6 mg, 0.12 mmol, 32%). **^{1}H NMR** (400 MHz, $CDCl_3$): δ 8.99 (s, 1H), 5.69 (s, 2H), 4.07 (dt, J = 11.4, 3.4 Hz, 2H), 3.97–3.88 (m, 4H), 3.80–3.74 (m, 4H), 3.58–3.49 (m, 2H), 2.92–2.82 (m, 1H), 2.03–1.87 (m, 4H). **^{19}F{^{1}H} NMR** (376 MHz, CDCl3): δ −65.29 (s, 3F). **^{13}C{^{1}H} NMR** (101 MHz, $CDCl_3$): δ 180.34 (s, 1C), 168.65 (s, 1C), 164.16 (s, 1C), 162.90 (s, 1C), 162.59 (s, 1C), 154.88 (q, J = 35.7 Hz, 1C), 120.55 (q, J = 276.5 Hz, 1C), 120.02 (s, 1C), 67.65 (s, 2C), 66.64 (s, 2C), 43.61 (s, 2C), 43.58 (s, 1C), 30.42 (s, 2C). **HRMS** (m/z): $[M + H]^+$ calc. for $C_{17}H_{21}F_3N_7O_2$ 412.1703; found: 412.1708. **HPLC** (ACN with 0.1% TFA): t_R = 6.47 min (96.63% purity).

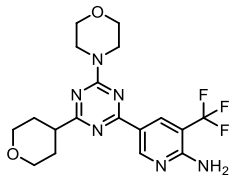

5-(4-morpholino-6-(tetrahydro-2*H*-pyran-4-yl)-1,3,5-triazin-2-yl)-3-(trifluoromethyl)pyridin-2-amine (5b) was prepared according to general procedure 4 from **5a** (92 mg, 0.20 mmol, 1.0 eq.). Purification by column chromatography on silica gel (cyclohexane/ethyl acetate 1:0 → 0:1) gave compound **5b** as a colourless solid (32.5 mg, 0.07 mmol, 35%). **^{1}H NMR** (400 MHz, $CDCl_3$): δ 9.25 (br s, 1H), 8.70 (br s, 1H), 5.34 (s, 2H), 4.11–4.03 (m, 2H), 3.95 (br s, 4H), 3.83–3.74 (m, 4H), 3.55 (td, J = 11.3, 3.2 Hz, 2H), 2.92–2.82 (m, 1H), 2.04–1.91 (m, 4H). **^{19}F{^{1}H} NMR** (376 MHz, $CDCl_3$): δ −64.16 (s, 3F). **^{13}C{^{1}H} NMR** (101 MHz, CDCl3): δ 180.32 (s, 1C), 168.42 (s, 1C), 164.51 (s, 1C), 156.84 (q, J = 1.4 Hz, 1C), 153.29–153.22 (m, 1C), 135.78 (q, J = 5.0 Hz, 1C), 124.13 (q, J = 271.7 Hz, 1C), 122.44 (s, 1C), 107.88 (q, J = 32.4 Hz, 1C), 67.72 (s, 2C), 66.74 (s, 2C), 43.68 (s, 1C), 43.57 (s, 2C), 30.58 (s, 2C). **HRMS** (m/z): $[M + H]^+$ calc. for $C_{18}H_{22}F_3N_6O_2$ 411.1751; found: 411.1758. **HPLC**: t_R = 8.79 min (96.66% purity).

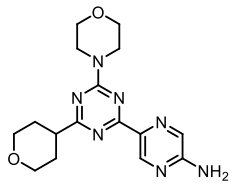

5-(4-morpholino-6-(tetrahydro-2*H*-pyran-4-yl)-1,3,5-triazin-2-yl)pyrazin-2-amine (6b) was prepared according to general procedure 4 from **6a** (80 mg, 0.23 mmol, 1.0 eq.). Purification by column chromatography on silica gel (cyclohexane/ethyl acetate 1:0 → 0:1) gave compound **6b** as a colourless solid (56.0 mg, 0.16 mmol, 70%). **^{1}H NMR** (400 MHz, $CDCl_3$): δ 9.69 (d, J = 1.6 Hz, 1H), 8.31 (dd, J = 2.6, 1.6 Hz, 1H), 8.24 (d, J = 2.6 Hz, 1H), 8.20 (br s, 1H), 4.08–4.01 (m, 2H), 3.97–3.81 (m, 4H), 3.78–3.72 (m, 4H), 3.55–3.45 (m, 2H), 2.82–2.71 (m, 1H), 2.02–1.88 (m, 4H). **^{13}C{^{1}H} NMR** (101 MHz, $CDCl_3$): δ 180.69 (s, 1C), 164.83 (s, 1C), 163.47 (s, 1C), 149.23 (s, 1C), 142.12 (s, 1C), 138.25 (s, 1C), 137.04 (s, 1C), 67.70 (s, 2C), 66.67 (s, 2C), 43.76 (s, 2C), 43.58 (s, 1C), 30.54 (s, 2C). **HRMS** (m/z): $[M + H]^+$ calc. for $C_{16}H_{22}N_7O_2$ 344.1829; found: 344.1835. **HPLC**: t_R = 6.75 min (95.81% purity).

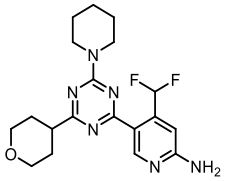

4-(difluoromethyl)-5-(4-(piperidin-1-yl)-6-(tetrahydro-2*H*-pyran-4-yl)-1,3,5-triazin-2-yl)pyridin-2-amine (7b) was prepared according to general procedure 4 from **7a** (140 mg, 0.36 mmol, 1.0 eq.). Purification by column chromatography on silica gel (cyclohexane/ethyl acetate 1:0 → 0:1) gave compound **7b** as a colourless solid (51.9 mg, 0.13 mmol, 37%). **^{1}H NMR** (400 MHz, $CDCl_3$): δ 8.94 (s, 1H), 7.74 (t, J = 55.3 Hz, 1H), 6.81 (s, 1H), 4.01 (dt, J = 11.2, 3.4 Hz, 2H), 3.86–3.76 (m, 4H), 3.57–3.43 (m, 2H), 3.05–2.99 (m, 2H), 2.83–2.72 (m, 1H), 1.98–1.86 (m, 4H), 1.73–1.51 (m, 6H). **^{19}F{^{1}H} NMR** (376 MHz, $CDCl_3$): δ −117.30 (s, 2F). **^{13}C{^{1}H} NMR** (101 MHz, $CDCl_3$): δ 179.64 (s, 1C), 169.53 (s, 1C), 163.86 (s, 1C), 160.50 (s, 1C), 152.03 (s, 1C), 144.07 (t, J = 22.1 Hz, 1C), 120.43 (t, J = 4.6 Hz, 1C), 111.33 (t, J = 239.0 Hz, 1C), 104.61 (t, J = 8.4 Hz, 1C), 67.78 (s, 2C), 44.34 (s, 2C), 43.54 (s, 1C), 30.48 (s, 2C), 25.73 (s, 2C), 24.69 (s, 1C). **HRMS** (m/z): $[M + H]^+$ calc. for $C_{19}H_{25}F_2N_6O$ 391.2052; found: 391.2058. **HPLC** (ACN with 0.1% TFA): t_R = 7.41 min (97.65% purity).

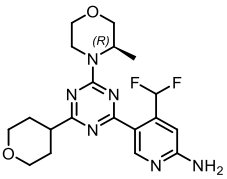

(*R*)-4-(difluoromethyl)-5-(4-(3-methylmorpholino)-6-(tetrahydro-2*H*-pyran-4-yl)-1,3,5-triazin-2-yl)pyridin-2-amine (8b) was prepared according to general procedure 4 from **8a** (227 mg, 0.56 mmol, 1.0 eq.). Purification by column chromatography on silica gel (cyclohexane/ethyl acetate 1:0 → 0:1) gave compound **8b** as a yellow solid (84 mg, 0.20 mmol, 37%). **^{1}H NMR** (400 MHz, $CDCl_3$): δ 9.11 (s, 1H), 7.82 (t, J = 55.3 Hz, 1H), 6.86 (s, 1H), 4.90 (s, 2H), 4.82 (br s, 1H), 4.51 (br s, 1H), 4.08 (dt, J = 11.4, 3.4 Hz, 2H), 4.01 (dd, J = 11.4, 3.8 Hz, 1H), 3.80 (d, J = 11.5 Hz, 1H), 3.70 (dd, J = 11.5, 3.3 Hz, 1H), 3.59–3.50 (m, 3H), 3.37–3.24 (m, 1H), 2.91–2.78 (m, 1H), 1.99–1.92 (m, 4H), 1.35 (d, J = 6.9 Hz, 3H). **^{19}F{^{1}H} NMR** (376 MHz, $CDCl_3$): δ −117.29 (s, 2F). **^{13}C{^{1}H} NMR** (101 MHz, CDCl3): δ 180.03 (s, 1C), 169.84 (s, 1C), 164.13 (s, 1C), 160.58 (s, 1C), 152.87 (s, 1C), 144.05 (t, J = 22.1 Hz, 1C), 120.56 (t, J = 4.7 Hz, 1C), 111.43 (t, J = 239.0 Hz, 1C), 104.30 (t, J = 8.4 Hz, 1C), 71.07 (s, 1C), 67.83 (s, 2C), 66.99 (s, 1C), 46.60 (s, 1C), 43.77 (s, 1C), 38.67 (s, 1C), 30.63 (s, 2C), 14.42 (s, 1C). **HRMS** (m/z): $[M + H]^+$ calc. for $C_{19}H_{25}F_2N_6O_2$ 407.2002; found: 407.2005. **HPLC**: t_R = 7.92 min (96.01% purity).

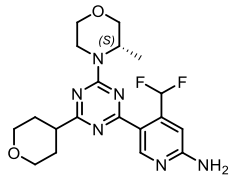

(*S*)-4-(difluoromethyl)-5-(4-(3-methylmorpholino)-6-(tetrahydro-2*H*-pyran-4-yl)-1,3,5-triazin-2-yl)pyridin-2-amine (9b) was prepared according to general procedure 4 from **9a** (198 mg, 0.49 mmol, 1.0 eq.). Purification by column chromatography on silica gel (cyclohexane/ethyl acetate 1:0 → 0:1) gave compound **9b** as a colourless solid (110 mg, 0.26 mmol, 55%). **^{1}H NMR** (400 MHz, $CDCl_3$): δ 9.10 (s, 1H), 7.81 (t, J = 55.3 Hz, 1H), 6.84 (s, 1H), 5.06 (s, 2H), 4.81 (br s, 1H), 4.50 (br s, 1H), 4.07 (dt, J = 11.4, 3.4 Hz, 2H), 4.00 (dd, J = 11.4, 3.8 Hz, 1H), 3.79 (d, J = 11.5 Hz, 1H), 3.69 (dd, J = 11.5, 3.3 Hz, 1H), 3.59–3.49 (m, 3H), 3.30 (td, J = 13.1, 3.7 Hz, 1H), 2.90–2.79 (m, 1H), 1.99–1.90 (m, 4H), 1.34 (d, J = 6.9 Hz, 3H). **^{19}F{^{1}H} NMR** (376 MHz, $CDCl_3$): δ −117.29 (s, 2F). **^{13}C{^{1}H} NMR** (101 MHz, $CDCl_3$): δ 179.92 (s, 1C), 169.73 (s, 1C), 164.02 (s, 1C), 160.48 (s, 1C), 152.76 (s, 1C), 143.93 (t, J = 22.0 Hz, 1C), 120.44 (t, J = 4.7 Hz, 1C), 111.32 (t, J = 239.0 Hz, 1C), 104.18 (t, J = 8.4 Hz, 1C), 70.96 (s, 1C), 67.72 (s, 2C), 66.88 (s, 1C), 46.49 (s, 1C), 43.66 (s, 1C), 38.56 (s, 1C), 30.52 (s, 2C), 14.31 (s, 1C). **HRMS** (m/z): $[M + H]^+$ calc. for $C_{19}H_{25}F_2N_6O_2$ 407.2002; found: 407.2005. **HPLC** (ACN with 0.1% TFA): t_R = 6.44 min (97.01% purity).

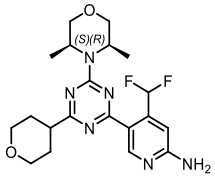

4-(difluoromethyl)-5-(4-((3*R*,5*S*)-3,5-dimethylmorpholino)-6-(tetrahydro-2*H*-pyran-4-yl)-1,3,5-triazin-2-yl)pyridin-2-amine (10b) was prepared according to general procedure 4 from **10a** (116 mg, 0.28 mmol, 1.0 eq.). Purification by column chromatography on silica gel (cyclohexane/ethyl acetate 1:0 → 0:1) gave compound **10b** as a colourless solid (49.4 mg, 0.12 mmol, 42%). **^{1}H NMR** (400 MHz, $CDCl_3$): δ 9.07 (s, 1H), 7.80 (d, J = 55.3 Hz, 1H), 6.84 (s, 1H), 4.68–4.56 (m, 2H), 4.05 (dt, J = 11.3, 3.4 Hz, 2H), 3.84 (d, J = 11.6 Hz, 2H), 3.65 (dd, J = 11.6, 3.9 Hz, 2H), 3.59–3.46 (m, 2H), 2.88–2.79 (m, 1H), 2.03–1.90 (m, 6H), 1.37 (d, J = 6.9 Hz, 6H). **^{19}F{^{1}H} NMR** (376 MHz, $CDCl_3$): δ −116.80 to −117.86 (m, 2F). **^{13}C{^{1}H} NMR** (101 MHz, $CDCl_3$): δ 179.81 (s, 1C), 169.65 (s, 1C), 163.69 (s, 1C), 160.50 (s, 1C), 152.58 (s, 1C), 144.10 (t, J = 22.1 Hz, 1C), 120.43 (t, J = 4.6 Hz, 1C), 111.37 (t, J = 239.1 Hz, 1C), 104.45 (t, J = 8.6 Hz, 1C), 71.37 (s, 2C), 67.81 (s, 2C), 45.96 (s, 2C), 43.62 (s, 1C), 30.56 (s, 2C), 18.98 (s, 2C). **HRMS** (m/z): $[M + H]^+$ calc. for $C_{20}H_{27}F_2N_6O_2$ 421.2158; found: 421.2164. **HPLC**: t_R = 9.01 min (98.04% purity).

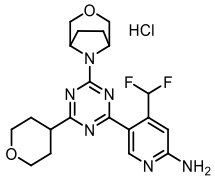

5-(4-(3-oxa-8-azabicyclo[3.2.1]octan-8-yl)-6-(tetrahydro-2*H*-pyran-4-yl)-1,3,5-triazin-2-yl)-4-(difluoromethyl)pyridin-2-amine HCl salt (11b) was prepared according to general procedure 4 from **11a** (1.0 g, 2.40 mmol, 1.0 eq.). Purification by column chromatography on silica gel (cyclohexane/ethyl acetate 1:0 → 0:1) gave the desired compound as a colourless solid (875 mg, 2.09 mmol, 87%). To a white suspension of the compound (830 mg, 1.99 mmol, 1.0 eq.) *in* methyl *tert*-butyl ether (10 mL), HCl in isopropanol (5–6 N, 600 μL, 2.98 mmol, 1.5 eq.) was slowly added. The suspension was stirred at room temperature for 6 h. The solid was filtered off and washed with methyl *tert*-butyl ether, dried in high vacuum to give compound **11b** (732 mg, 1.61 mmol, 81%) as a colourless solid. **^{1}H NMR** (400 MHz, DMSO-d_6): δ 8.91 (s, 1H), 7.86 (t, J c = 54.4 Hz, 1H), 7.17 (s, 1H), 4.78–4.69 (m, 2H), 3.98–3.88 (m, 2H), 3.72–3.56 (m, 4H), 3.44 (td, J = 11.4, 2.5 Hz, 2H), 2.84 (tt, J = 11.2, 4.1 Hz, 1H), 2.11–1.69 (m, 8H). **^{19}F{^{1}H} NMR** (400 MHz, DMSO-d_6): δ −117.29 (s, 2F). **^{13}C{^{1}H} NMR** (101 MHz, DMSO-d_6): δ 180.38 (s, 1C), 167.97 (s, 1C), 161.78 (s, 1C), 156.85 (s, 1C), 146.28 (s, 1C), 143.31 (br s, 1C), 118.58 (br s, 1C), 111.34 (t, J = 239.0 Hz, 1C), 110.04 (t, J = 9.0 Hz, 1C), 71.48 (s, 2C), 67.04 (s, 2C), 55.10 (s, 1C), 55.05 (s, 1C), 43.21 (s, 1C), 30.56 (s, 1C), 30.48 (s, 1C), 26.79 (s, 1C), 26.71 (s, 1C). **HRMS** (m/z): $[M + H]^+$ calc. for $C_{20}H_{25}F_2N_6O_2$ 419.2002; found: 419.2002. **HPLC**: t_R = 7.81 min (>99% purity). M.p. 240–250 °C (dec).

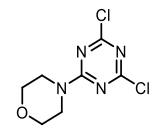

4-(4,6-dichloro-1,3,5-triazin-2-yl)morpholine (12). Compound **12** was prepared according to the literature [43].

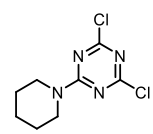

2,4-dichloro-6-(piperidin-**1-yl)-1,3,5-triazine (13).** Compound **13** was prepared according to the literature [49].

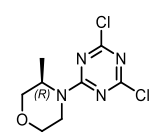

(*R*)-4-(4,6-dichloro-1,3,5-triazin-2-yl)-3-methylmorpholine (14). Compound **14** was prepared according to the literature [49].

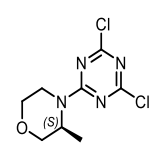

(*S*)-4-(4,6-dichloro-1,3,5-triazin-2-yl)-3-methylmorpholine (15). Compound **15** was prepared according to the literature [49].

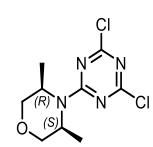

(3*R*,5*S*)-4-(4,6-dichloro-1,3,5-triazin-2-yl)-3,5-dimethylmorpholine (16). Compound **16** was prepared according to the literature [25].

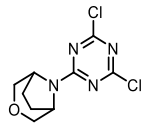

8-(4,6-dichloro-1,3,5-triazin-2-yl)-3-oxa-8-azabicyclo [3.2.1] octane (17). Compound **17** was prepared according to the literature [26].

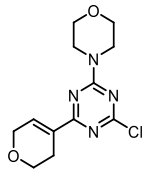

4-(4-chloro-6-(3,6-dihydro-2*H*-pyran-4-yl)-1,3,5-triazin-2-yl) morpholine (18). Compound **18** was prepared according to general procedure 1 from 3,6-dihydro-2*H*-pyran-4-boronic acid pinacol ester (3.0 g, 14.0 mmol, 1.1 eq.) and intermediate **12** (3.0 g, 13.0 mmol, 1.0 eq.). Purification by column chromatography on silica gel (cyclohexane/ethyl acetate 1:0 → 9:1) gave compound **18** as a colourless solid (2.1 g, 7.43 mmol, 57%). **^{1}H NMR** (400 MHz, $CDCl_3$): δ 7.39–7.35 (m, 1H), 4.38 (q, J = 2.8 Hz, 2H), 3.94–3.90 (m, 2H), 3.89–3.84 (m, 4H), 3.79–3.72 (m, 4H), 2.60–2.53 (m, 2H). **MALDI-MS**: m/z = 283.698 $[M + H]^+$.

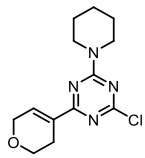

2-chloro-4-(3,6-dihydro-2*H*-pyran-4-yl)-6-(piperidin-1-yl)-1,3,5-triazine (19). Compound **19** was prepared according to general procedure 1 from 3,6-dihydro-2*H*-pyran-4-boronic acid pinacol ester (901 mg, 4.30 mmol, 1.0 eq.) and compound **13** (1.0 g, 4.30 mmol, 1.0 eq.). Purification by column chromatography on silica gel (cyclohexane/ethyl acetate 1:0 → 9:1) gave compound **19** as a colourless solid (419 mg, 1.49 mmol, 35%). **^{1}H NMR** (400 MHz, $CDCl_3$): δ 7.36–7.31 (m, 1H), 4.37 (q, J = 2.8 Hz, 2H), 3.89–3.84 (m, 4H), 3.83–3.78 (m, 2H), 2.62–2.55 (m, 2H), 1.75–1.67 (m, 2H), 1.66–1.58 (m, 4H). **MALDI-MS**: 281.752 m/z = $[M + H]^+$.

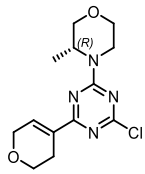

(*R*)-4-(4-chloro-6-(3,6-dihydro-2*H*-pyran-4-yl)-1,3,5-triazin-2-yl)-3-methylmorpholine (20). Compound **20** was prepared according to general procedure 1 from 3,6-dihydro-2*H*-pyran-4-boronic acid pinacol ester (850 mg, 4.07 mmol, 1.0 eq.) and compound **14** (1.0 g, 4.07 mmol, 1.0 eq.). Purification by column chromatography on silica gel (cyclohexane/ethyl acetate 1:0 → 9:1) gave compound **20** as a colourless solid (456 mg, 1.54 mmol, 38%). **^{1}H NMR** (400 MHz, $CDCl_3$): δ 7.36 (s, 1H), 4.86–4.70 (m, 1H), 4.54–4.34 (m, 1H), 4.38 (q, J = 2.8 Hz, 2H), 3.98 (dd, J = 11.6, 3.8 Hz, 1H), 3.87 (t, J = 5.5 Hz, 2H), 3.77 (d, J = 11.7 Hz, 1H), 3.66 (dd, J = 11.7, 3.2 Hz, 1H), 3.51 (td, J = 12.0, 2.9 Hz, 1H), 3.32 (td, J = 13.1, 3.8 Hz, 1H), 2.60–2.53 (m, 2H), 1.35 (d, J = 6.9 Hz, 3H). **MALDI-MS**: m/z = 297.671 $[M + H]^+$.

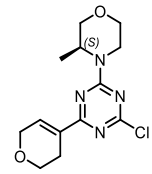

(*S*)-4-(4-chloro-6-(3,6-dihydro-2*H*-pyran-4-yl)-1,3,5-triazin-2-yl)-3-methylmorpholine (21). Compound **21** was prepared according to general procedure 1 from 3,6-dihydro-2*H*-pyran-4-boronic acid pinacol ester (850 mg, 4.07 mmol, 1.0 eq.) and compound **15** (1.0 g, 4.07 mmol, 1.0 eq.). Purification by column chromatography on silica gel (cyclohexane/ethyl acetate 1:0 → 9:1) gave compound **21** as a colourless solid (422 mg, 1.42 mmol, 35%). **^{1}H NMR** (400 MHz, $CDCl_3$): δ 7.37 (s, 1H), 4.86–4.71 (m, 1H), 4.56–4.36 (m, 1H), 4.38 (q, J = 2.9 Hz, 2H), 3.99 (dd, J = 11.6, 3.8 Hz, 1H), 3.87 (t, J = 5.4 Hz, 2H), 3.77 (d, J = 11.6 Hz, 1H), 3.66 (dd, J = 11.6, 3.3 Hz, 1H), 3.57-c3.46 (m, 1H), 3.32 (td, J = 13.0, 3.8 Hz, 1H), 2.61–2.53 (m, 2H), 1.35 (d, J = 6.9 Hz, 3H). **MALDI-MS**: m/z = 297.704 $[M + H]^+$.

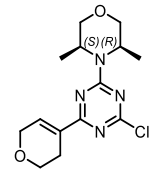

(3*R*,5*S*)-4-(4-chloro-6-(3,6-dihydro-2*H*-pyran-4-yl)-1,3,5-triazin-2-yl)-3,5-dimethylmorpholine (22). Compound **22** was prepared according to general procedure 1 from 3,6-dihydro-2*H*-pyran-4-boronic acid pinacol ester (798 mg, 3.80 mmol, 1.0 eq.) and compound **16** (1.0 g, 3.80 mmol, 1.0 eq.). Purification by column chromatography on silica gel (cyclohexane/ethyl acetate 1:0 → 8:2) gave compound **22** as a colourless solid (462 mg, 1.48 mmol, 39%). **^{1}H NMR** (400 MHz, $CDCl_3$): δ 7.38–7.35 (m, 1H), 4.60 (br s, 2H), 4.38 (q, J = 2.9 Hz, 2H), 3.87 (t, J = 5.5 Hz, 2H), 3.84 (d, J = 11.6 Hz, 2H), 3.64 (dd, J = 11.6, 3.9 Hz, 2H), 2.60–2.53 (m, 2H), 1.39 (d, J = 7.0 Hz, 6H). **HPLC-MS**: m/z = 311.1872 $[M + H]^+$.

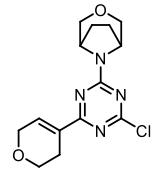

(1*R*,5*S*)-8-(4-chloro-6-(3,6-dihydro-2*H*-pyran-4-yl)-1,3,5-triazin-2-yl)-3-oxa-8-azabicyclo [3.2.1] octane (23). Compound **23** was prepared according to general procedure 1 from 3,6-dihydro-2*H*-pyran-4-boronic acid pinacol ester (563 mg, 2.68 mmol, 1.0 eq.) and compound **17** (700 mg, 2.68 mmol, 1.0 eq.). Purification by column chromatography on silica gel (cyclohexane/ethyl acetate 1:0 → 9:1) gave compound **23** as a colourless solid (372 mg, 1.21 mmol, 45%). **^{1}H NMR** (400 MHz, $CDCl_3$): δ 7.37–7.34 (m, 1H), 4.81–4.69 (m, 2H), 4.37 (q, J = 2.8 Hz, 2H), 3.86 (t, J = 5.5 Hz, 2H), 3.77–3.64 (m, 4H), 2.56 (ttd, J = 5.5, 2.8, 1.6 Hz, 2H), 2.17–1.97 (m, 4H). **HPLC-MS**: m/z = 309.1844 $[M + H]^+$.

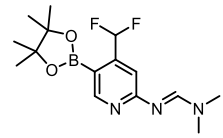

***N*'- [4-(Difluoromethyl)-5-(4,4,5,5-tetramethyl-1,3,2-dioxaborolan-2-yl)pyridin-2-yl] -*N*,*N*-dimethylmethanimidamide (24).** Compound **24** was prepared according to the literature [26,65].

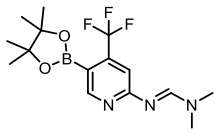

(*E*)-*N*,*N*-dimethyl-*N*'-(5-(4,4,5,5-tetramethyl-1,3,2-dioxaborolan-2-yl)-4-(trifluoromethyl)pyridin-2-yl)formimidamide (25). Compound **25** was prepared according to the literature [43].

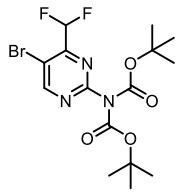

***tert*-butyl (5-bromo-4-(difluoromethyl)pyrimidin-2-yl)(*tert*-butoxycarbonyl)carbamate (26).** Compound **26** was prepared according to the literature [47].

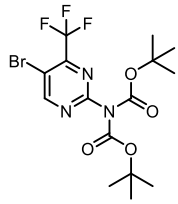

***tert*-butyl (5-bromo-4-(trifluoromethyl)pyrimidin-2-yl)(*tert*-butoxycarbonyl)carbamate (27).** Compound **27** was prepared according to literature [47].

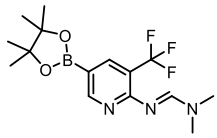

(*E*)-*N*,*N*-dimethyl-*N*'-(5-(4,4,5,5-tetramethyl-1,3,2-dioxaborolan-2-yl)-3-(trifluoromethyl)pyridin-2-yl)formimidamide (28). Compound **28** was prepared according to the literature [30].

5.4. General bioassay procedures

5.4.1. Determination of inhibitor dissociation constants

Dissociation constants of compounds (K_i) for p110α and mTOR were determined using a commercial LanthaScreen (Life Technologies) assay. The assays were performed as described in Ref. [44], and data analysis was carried out as previously reported in Ref. [43]. Briefly, AlexaFluor647-labeled Kinase Tracer314 (#PV6087) with a K_d of 2.2 nM was used at 20 nM for p110α and at a final concentration of 10 nM for mTOR (K_d of 19 nM). Recombinant N-terminally $(His)_6$-tagged p110α was captured with biotinylated anti-$(His)_6$-tag antibody (2 nM, #PV6089) and detected with LanthaScreen Eu-steptavidin (2 nM, #PV5899); *N*-terminal GST fused to truncated mTOR (amino acids 1360–2549; #PR8683B) was detected with a LanthaScreen Eu-labeled anti-GST antibody (2 nM, #PV5594). The p110α assay buffer was composed of 50 mM HEPES pH 7.5, 10 mM $MgCl_2$, 1 mM EGTA, and 0.01% (v/v) Brij-35, and the mTOR assay buffer contained 50 mM HEPES; 5 mM $MgCl_2$; 1 mM EGTA; 0.01% Pluronic F-127. IC_{50}s were measured using a 10-point 1:4 serial dilution. Values at each concentration were determined in independent duplicate experiments.

5.4.2. Structure modeling of mTOR kinase complexes

The coordinates of mTOR kinase bound to PI103 (PDB code 4JT6; 3.6 Å) were used as starting points for docking the molecules into the kinase ATP-binding site. Compounds were manually replaced/modified in crystal structures using Maestro 11.1 and energy minimization of the resulting protein-inhibitor complex was carried out. Measurements and Fig.s were generated using Maestro Schrödinger 11.1 and Pymol Schrödinger 2.5.2.

5.4.3. Small-molecule single-crystal X-ray diffraction

Single crystal data for compound **11b** were collected at 150K on a STOE StadiVari Eulerian 4-circle diffractometer (CuKα radiation) equipped with a Dectris Eiger2 1 M detector Single crystal data for compound **11a** were collected at 150K on a STOE StadiVari Eulerian 4-circle diffractometer (GaK*α* radiation, MetalJet source) equipped with a Dectris PILATUS 300K detector. Both structures were solved using Superflip [66,67] and Olex2 [68]. The model was refined with ShelXL v. 2018/3 [69]. All H atoms were included at geometrically calculated positions and refined using a riding model with Uiso = 1.2 of the parent atom. Structure analysis and structural diagrams used CSD Mercury 2022.2.0 [70]. For compound **11a** a solvent mask was used to treat part of the solvent region and electrons removed corresponded to 0.75 ethyl acetate per formula unit.

5.4.4. Kinome profiling

The inhibitory capacity and selectivity of compound was determined using the KdELECT platform provided by DiscoverX [71]. In short, binding of immobilized ligand to DNA-tagged kinases was competed with 10 μM compound. The amount of kinase bound to the immobilized ligand was measured by quantitative PCR of the respective DNA tags and is given as percentage of control. Binding constants of compounds for kinases of interest were determined by competing the immobilized ligand kinase interactions with an 11-point 3-fold serial dilution of compound starting from 30 μM and subsequent quantitative PCR of DNA tags. Binding constants were calculated by a standard dose-response curve using the Hill equation (with Hill Slope set to −1):

Response = Background + (Signal - Background)/(1 + 10^([lg Kd - lg dose] * HillSlope))

Selectivity cores [72] were calculated as

S = Number of hits / Number of tested kinases (excluding mutant variants)

where S35, S10, S1 were calculated using %Ctrl as a potency threshold (35, 10, 1%); for example

S(35) = (number of non-mutant kinases with %Ctrl <35)/(number of non-mutant kinases tested)

5.4.5. Cellular PI3K and mTOR signaling

The SKOV3 human ovarian cancer cell line harbors a PI3Kα H1047R mutation and upregulates expression of HER2 receptors, which results in a robust activation of the PI3K/mTOR signaling pathway. This yields an excellent signal-to-noise ratio in in-cell western (ICW) assays and provides reproducible readouts for phosphorylated ribosomal protein S6 (pS6) downstream of TORC1 and TORC2-dependent phosphorylation of PKB/Akt on Ser473 (pPKB/Akt). Therefore, SKOV3 cells are well suited for SAR studies on inhibitors targeting the PI3K/mTOR pathway.

The assays were performed as previously described in Ref. [29]. Briefly, in-cell western (ICW) assays were used to measure phosphorylation of PKB/Akt at Ser473 and phosphorylation of ribosomal protein

S6 at Ser235/236. ICW experiments and determination of IC_{50} were performed as described in ref (30). Briefly, SKOV3 cells were seeded at 1.2×10^4 cells/well in 96-well plates (Cell Carrier, PerkinElmer) and grown for 24 h at 37 °C (at 5% CO_2). Cells were then exposed to inhibitors or DMSO for and incubated for 1 h at 37 °C (at 5% CO_2). Then, cells were fixed (4% PFA in PBS for 30 min at room temperature), blocked with a blocking solution (1% BSA/0.1% Triton X-100/5% goat serum in PBS) for 30 min at room temperature, and stained overnight at 4 °C with either a primary antibody to detect phosphorylation of Ser473 of PKB/Akt [rabbit monoclonal antibody from Cell Signaling Technology (CST), #4058, diluted 1:500 in blocking solution) or a primary antibody to detect phosphorylation of Ser235/236 of the ribosomal protein S6 [rabbit monoclonal antibody from CST, #4856, diluted 1:500 in blocking solution]. Tubulin staining was assessed together with one of the anti-phosphoprotein antibodies as the internal standard with mouse anti-α-tubulin, 1:2000, from Sigma (#T9026). Fluorescence outputs were detected on an Odyssey CLx infrared imaging scanner (LICOR) using secondary, species-specific antibodies, IR-dye-labeled antibodies (IRDye680-conjugated goat anti-mouse, and IRDye800-conjugated goat anti-rabbit antibodies [LICOR # 926–68070 and # 926–32211], both diluted 1:500 in 1%BSA/0.1% Triton X-100 in PBS). Remaining phospho-protein signals were normalized to cellular tubulin and related to DMSO controls. IC_{50}s were measured using a 11-point 1:2 serial dilution and each concentration was measured in independent duplicate.

5.4.6. Hepatocyte stability assay

The assays were performed as previously described in Ref. [29]. Briefly, primary hepatocytes from mouse (CD-1), rat (Sprague-Dawley, SD), dog (Beagle), and human were used. Assays were performed using cryopreserved hepatocytes in suspension. Hepatocytes were thawed according to the instructions of the supplier before seeding in 48-well cell culture plates at a density of 200,000 cells/well in 225 μl incubation medium consisting of WME (Williams Medium E) supplemented with 2 mM L-glutamine and 25 mM HEPES. Stock solution of compound **11b** was prepared with 10 mM in DMSO. A working solution was obtained by dilution of the stock solution in DMSO (first step) and in incubation medium (second step) resulting in a concentration of 10-fold higher strength (50 μM) than the final intended test concentration (5 μM) and a solvent content of 5% DMSO.

Positive control incubations were performed using 7-ethoxycoumarin as substrate. A 10 mM stock solution in acetonitrile (ACN) was further diluted in ACN (first step) and in incubation medium (second step) to give a working solution in 10% ACN and of 10-fold higher strength than the final intended incubation concentration (5 μM). To 225 μL of cell suspension, 25 μL of the 10-fold concentrated working solution of test or reference item was added, resulting in a final test concentration of 5 μM for compound **11b** or 7-ethoxycoumarin, respectively, with final solvent concentrations of 0.5% DMSO (**11b**) or 1% ACN (7-ethoxycoumarin). For analysis, samples were taken after 0, 15, 60, 90 and 180 min of incubation for compound **11b** and after 0, 60 and 180 min for reference item. The sample preparation was performed afterwards by protein precipitation using ACN (200 μL cell suspension plus 200 μL ACN/ISTD3). After centrifugation (5 min, 4,800×*g*), the particle-free supernatants were diluted with one volume water and were analyzed by LC-MS. Negative controls were performed to exclude non-metabolic degradation processes; i.e. the finding that the concentrations remained stable over the investigated time suggests that the decrease of the parent compound was mainly due to metabolism. Negative control incubations were performed in line with all experiments using incubation medium in absence of hepatocytes.

For quantitative analysis of compound **11b** in samples from primary human hepatocytes, the HPLC system consisted of a LC pump Surveyor Plus and an auto sampler Surveyor Plus (Thermo-Fisher, USA). Mass spectrometry was performed on a TSQ Quantum Discovery Max triple quadrupole mass spectrometer equipped with an electro-spray ion source (ESI) (Thermo Fisher Scientific, USA) connected to a PC running the standard software Xcalibur 2.0.7.

5.4.7. CYP reactive phenotyping with human recombinant CYP1A1 and CYP1A2 isoenzymes

The assays were performed as previously described in Ref. [29]. Briefly, human recombinant isoenzymes from insect cells infected by baculovirus and containing cDNA of a single human CYP isoenzyme (Supersomes™, Corning) were used. The test item stock solutions were diluted in DMSO/H2O (1:8, v/v) to obtain 50-fold concentrated working solutions (solvent content 12.5% DMSO/87.5% H_2O) for CYP1A1 and CYP1A2. The test compound concentration applied in the CYP reactive phenotyping assay was 1 μM in presence of 0.25% DMSO. The assays were performed in duplicate using human recombinant enzymes systems from Corning (BD Gentest P450 High Throughput Inhibitor Screening Kits). The cofactor-mix, containing the NADP + -regenerating system, was prepared according to the instructions of the manufacturer. For CYP1A1 and CYP1A2, 4 μL of the 50-fold concentrated working solution was added to 96 μL cofactor-mix. Cofactor mix and test item were pipetted into the respective wells of a pre-warmed 96-well-plate and pre-warmed for 10 min on a shaker with fitted heating block. The reactions were initiated by addition of 100 μL pre-warmed enzyme-mix. By default, the final protein concentration of all CYP isoenzymes was 25 pmol/mL. Incubations with a final volume of 200 μL were performed at 37 °C. After 0 and 60 min (30 min for positive control substrates), the reactions were stopped by the addition of 200 μL stop solution, i.e. ACN containing the internal standard. Two control groups were run in parallel for every assay: positive controls (PC, n = 2) using specific probe substrates for each CYP isoform as reference compounds (CYP1A1 = Melatonin and CYP1A2 = Phenacetin) to prove the quality of the enzyme activity of the used batches as well as a negative control (NC, n = 2), which were performed without cofactors and glucose-6-phosphate-dehydrogenase to ensure that the potential loss of parent compound is due to CYP-mediated metabolism.

For quantitative analysis of compound **11b**, LC-MS systems were used: (i) LC-MS: Accela U-HPLC pump and an Accela auto sampler (Thermo Fisher Scientific, USA) connected to an Exactive mass spectrometer (Orbitrap with accurate mass (Thermo Fisher Scientific, USA)); data handling with the standard software Xcalibur 2.1; (ii) LC-HRMS: Accela U-HPLC pump and an Accela Open auto sampler (Thermo Fisher Scientific, USA) connected to an Q-Exactive mass spectrometer (Orbitrap); data handling with the standard software Xcalibur 2.2. (iii) LC-MS: Surveyor MS Plus HPLC (Thermo Electron) HPLC system connected to a TSQ Quantum Discovery Max (Thermo Electron) triple quadrupole mass spectrometer equipped with an electrospray (ESI) or APCI interface (Thermo Fisher Scientific, USA); connected to a PC running the standard software Xcalibur 2.0.7.

The pump flow rate was set to 600 μL/min and the analytes were separated on a Kinetex Phenyl-Hexyl analytical column 2.6 μm, 50 × 2.1 mm (Phenomenex, Germany).

5.4.8. Pharmacokinetic studies in male Sprague Dawley rats

The assays were performed as previously described in Ref. [29]. Briefly, male Sprague Dawley rats (8 weeks old at delivery) were purchased from Janvier Labs (France). The animals were housed in a temperature-controlled room (20–24 °C) and maintained in a 12 h light/12 h dark cycle. Food and water were available *ad libitum* throughout the duration of the study. Formulation of compound **11b** was prepared by weighing the test items into glass vials and dissolving them by addition of Captisol (40% w/w in water) and water for injection in a proportion of 50% and 35% of the final desired volume. The pH was adjusted to 3 with 0.2 M HCl and finally, the volume was completed with water for injection. The formulations were stirred continuously until application to the animals. The compound was administrated orally at 5 mg/kg (application volume: 5 mL/kg) in 20% Captisol. At each time point (30 min, 2, 4 and 8 h), three rats were anesthetized with isoflurane

and 1 mL blood was collected, via heart puncture, in tubes containing lithium-heparin. After blood sampling, the rats were euthanized and brain, liver and skin were collected. Blood samples were stored on dry ice until centrifugation at 6000 rpm (10 min, 4 °C). Plasma supernatants and tissue samples were kept at −80 °C until being assayed. The calibration standards and quality controls were prepared in duplicates. A volume of 50 μL of unknown samples, zero samples and blanks were spiked with 6 μL DMSO. After 10 min of equilibration, a volume of 100 μL acetonitrile containing the internal standard (Diazepam, 300 ng/mL) was added to each calibration standard, QC, zero sample and unknown sample, while a volume of 100 μL plain acetonitrile was added to all blanks. Samples were vigorously shaken and centrifuged for 10 min at 6000 g and 20 °C. The particle free supernatant was diluted 1 + 1 with water. An aliquot was transferred to 200 μL sampler vials and subsequently subjected to LC-MS. The HPLC system consisted of an Accela U-HPLC pump and an Accela auto sampler (Thermo Fisher Scientific, USA). Mass spectrometry was performed on an Exactive mass spectrometer (orbitrap technology with accurate mass) equipped with a heated electrospray (H-ESI 2) interface (Thermo Fisher Scientific, USA) connected to a PC running the standard software Xcalibur 2.1.

Quantification of Plasma Insulin. Plasma insulin was determined using an immunoassay kit (Rat/Mouse Insulin ELISA from Merck Millipore, cat. no. EZRMI-13K, lot 2688510, Germany), according to the manufacturer's instructions.

Quantification of Plasma Glucose. Plasma glucose was determined using a glucose colorimetric assay (Cayman, cat. No. 10009582, lot 0478964, USA).

Ethic statement: all experimental procedures were approved by and conducted in accordance with the regulations of the local Animal Welfare authorities (Landesamt für Gesundheit und Verbraucherschutz, Abteilung Lebensmittel-und Veterinärwesen, Saarbrücken).

5.4.9. Cell lines

Lymphoma cell lines were cultured according to the recommended conditions, using RPMI-1640 medium, supplemented with 10% (v/v) fetal bovine serum (FBS), Penicillin-Streptomycin (~5,000 units penicillin and 5 mg streptomycin, Sigma) and L-glutamine (1%). Cell line identities were validated with the Promega GenePrint 10 System kit, and all experiments with the cells were performed within one month of their being thawed. Cells were periodically tested to confirm Mycoplasma negativity using the MycoAlert Mycoplasma Detection Kit (Lonza). Cells were incubated at 37 °C with 5% CO_2 and were subcultured every three days.

5.4.10. Compounds for in vitro screening

All compounds (powder) were dissolved in dimethyl sulfoxide (DMSO) to obtain a stock concentration of 10 mM and were stored frozen at −20 °C. The DMSO concentration did not exceed 0.1% in any experiment.

5.4.11. Cell proliferation analysis

Cells were seeded into 96-well plates (non-tissue culture treated) at a density of 10,000 cells/well. Cells were tested with increasing doses of the compounds ranging from 0 to 10 μM, and IC_{50} values were calculated. These assays were performed in duplicate. Wells containing medium only were included on each plate and used as blanks for absorbance readings.

MTT (Sigma, Buchs) was prepared as a 5 mg/mL stock in phosphate-buffered saline (PBS) and filter-sterilized. After 72 h, 20 μL of MTT solution was added to each well, and microplates were incubated at 37 °C for 4 h. Cells were then lysed with 50 μL of 25% sodium dodecyl sulfate, and absorbance was read at 570 nm using a Cytation plate reader.

Author contributions

The manuscript was written with contribution of all authors. All authors have given approval to the final version of the manuscript.

Funding sources

This work was supported by the Swiss National Science Foundation grants 310030_153211, 316030_133860, SNF 316030_198526 and 200021_204602; a Swiss Cancer Research KFS-5442-08-2021 grant and the Stiftung für Krebsbekämpfung grant 341 (to M.P.W.).

Declaration of competing interest

The authors declare the following financial interests/personal relationships which may be considered as potential competing interests: Matthias P. Wymann reports financial support was provided by Swiss National Science Foundation and by Swiss Cancer Research Foundation. Matthias P. Wymann, Martina De Pascale and Chiara Borsari have a patent on dihydropyran- and tetrahydropyran-substituted triazines pending to University of Basel, Tech. Transfer Office, Unitectra.

Data availability

Accesion codes are available for the readers.

Acknowledgements

We thank Anna Melone and Maja Wolleb for contribution to biological testing; and Alix Dall'Asen for contributions to synthetic efforts; Michael Pfeffer and the mass spectrometry team at the University of Basel for HRMS data. C.B. thanks L'Oréal Italy for Women and Science in collaboration with Italy's National Commission for UNESCO for the "L'Oréal Italia for Women in Science" fellowship.

Appendix A. Supplementary data

Supplementary data to this article can be found online at https://doi.org/10.1016/j.ejmech.2022.115038.

Abbreviations

mTOR	mechanistical (or mammalian) target of Rapamycin
TORC1	mTOR complex 1
TORC2	mTOR complex 2
PI3K	phosphoinositide 3-kinase
PKB	protein kinase B/Akt
S6K	p70 S6 kinase
DHP	3,6-dihydro-2*H*-pyran
THP	tetrahydro-2*H*-pyran
SAR	Structure-Activity Relationship
PK	pharmacokinetic
PD	pharmacodynamic
TR-FRET	time-resolved Förster resonance energy transfer
MALDI-ToF	Matrix-assisted laser desorption/ionization (MALDI) with the flight analysis (Time of Flight, ToF)
TSC1	hamartin
TSC2	tuberin
TSC	tuberous sclerosis complex

References

[1] M.P. Wymann, R. Schneiter, Lipid signalling in disease, Nat. Rev. Mol. Cell Biol. 9 (2008) 162–176.
[2] C. Borsari, M.P. Wymann, Targeting phosphoinositide 3-kinase - five decades of chemical space exploration, Chimia 75 (2021) 1037–1044.
[3] M.P. Wymann, R. Marone, Phosphoinositide 3-kinase in disease: timing, location, and scaffolding, Curr. Opin. Cell Biol. 17 (2005) 141–149.
[4] D.D. Sarbassov, D.A. Guertin, S.M. Ali, D.M. Sabatini, Phosphorylation and regulation of Akt/PKB by the rictor-mTOR complex, Science 307 (2005) 1098–1101.
[5] B. Magnuson, B. Ekim, D.C. Fingar, Regulation and function of ribosomal protein S6 kinase (S6K) within mTOR signalling networks, Biochem. J. 441 (2012) 1–21.
[6] R.A. Saxton, D.M. Sabatini, mTOR signaling in growth, metabolism, and disease, Cell 168 (2017) 960–976.
[7] Z. Zou, T. Tao, H. Li, X. Zhu, mTOR signaling pathway and mTOR inhibitors in cancer: progress and challenges, Cell Biosci. 10 (2020) 31.
[8] X. Wu, Y. Xu, Q. Liang, X. Yang, J. Huang, J. Wang, H. Zhang, J. Shi, Recent advances in dual PI3K/mTOR inhibitors for tumour treatment, Front. Pharmacol. 13 (2022), 875372.
[9] Z.Z. Chong, Y.C. Shang, S. Wang, K. Maiese, A critical kinase cascade in neurological disorders: PI 3-K, Akt, and mTOR, Future Neurol. 7 (2012) 733–748.
[10] J. Choi, J. Chen, S.L. Schreiber, J. Clardy, Structure of the FKBP1 2-rapamycin complex interacting with the binding domain of human FRAP, Science 273 (1996) 239–242.
[11] H.J. Eisen, E.M. Tuzcu, R. Dorent, J. Kobashigawa, D. Mancini, H.A. Valantine-von Kaeppler, R.C. Starling, K. Sørensen, M. Hummel, J.M. Lind, K.H. Abeywickrama, P. Bernhardt, Everolimus for the prevention of allograft rejection and vasculopathy in cardiac-transplant recipients, N. Engl. J. Med. 349 (2003) 847–858.
[12] L.H. Meng, X.F. Zheng, Toward rapamycin analog (rapalog)-based precision cancer therapy, Acta Pharmacol. Sin. 36 (2015) 1163–1169.
[13] V.E. Kwitkowski, T.M. Prowell, A. Ibrahim, A.T. Farrell, R. Justice, S.S. Mitchell, R. Sridhara, R. Pazdur, FDA approval summary: temsirolimus as treatment for advanced renal cell carcinoma, Oncol. 15 (2010) 428–435.
[14] G. Jerusalem, A. Rorive, J. Collignon, Use of mTOR inhibitors in the treatment of breast cancer: an evaluation of factors that influence patient outcomes, Breast Cancer 6 (2014) 43–57.
[15] A.S. Don, X.F. Zheng, Recent clinical trials of mTOR-targeted cancer therapies, Rev. Recent Clin. Trials 6 (2011) 24–35.
[16] Z. Zhang, Q. Fan, X. Luo, K. Lou, W.A. Weiss, K.M. Shokat, Brain-restricted mTOR inhibition with binary pharmacology, Nature 609 (2022) 822–828.
[17] M. Wymann, C. Borsari, Two-drug trick to target the brain blocks toxicity in the body, Nature 609 (2022) 681–683.
[18] C. Borsari, M. De Pascale, M.P. Wymann, Chemical and structural strategies to selectively target mTOR kinase, ChemMedChem 16 (2021) 2744–2759.
[19] E.K. Slotkin, P.P. Patwardhan, S.D. Vasudeva, E. de Stanchina, W.D. Tap, G. K. Schwartz, MLN0128, an ATP-competitive mTOR kinase inhibitor with potent in vitro and in vivo antitumor activity, as potential therapy for bone and soft-tissue sarcoma, Mol. Cancer Therapeut. 14 (2015) 395–406.
[20] D.S. Mortensen, K.E. Fultz, S. Xu, W. Xu, G. Packard, G. Khambatta, J.C. Gamez, J. Leisten, J. Zhao, J. Apuy, K. Ghoreishi, M. Hickman, R.K. Narla, R. Bissonette, S. Richardson, S.X. Peng, S. Perrin-Ninkovic, T. Tran, T. Shi, W.Q. Yang, Z. Tong, B. E. Cathers, M.F. Moghaddam, S.S. Canan, P. Worland, S. Sankar, H.K. Raymon, CC-223, a potent and selective inhibitor of mTOR kinase: in vitro and in vivo characterization, Mol. Cancer Therapeut. 14 (2015) 1295–1305.
[21] K.G. Pike, K. Malagu, M.G. Hummersone, K.A. Menear, H.M. Duggan, S. Gomez, N. M. Martin, L. Ruston, S.L. Pass, M. Pass, Optimization of potent and selective dual mTORC1 and mTORC2 inhibitors: the discovery of AZD8055 and AZD2014, Bioorg. Med. Chem. Lett 23 (2013) 1212–1216.
[22] Calithera Biosciences, Calithera Receives FDA Fast Track Designation for Sapanisertib for the Treatment of NRF2-Mutated Squamous Lung Cancer, News Release, 2022.
[23] X.Y. Luo, K.M. Wu, X.X. He, Advances in drug development for hepatocellular carcinoma: clinical trials and potential therapeutic targets, J. Exp. Clin. Cancer Res. 40 (2021) 172.
[24] L.A. Banaszynski, C.W. Liu, T.J. Wandless, Characterization of the FKBP. rapamycin.FRB ternary complex, J. Am. Chem. Soc. 127 (2005) 4715–4721.
[25] C. Borsari, E. Keles, D. Rageot, A. Treyer, T. Bohnacker, L. Bissegger, M. De Pascale, A. Melone, R. Sriramaratnam, F. Beaufils, M. Hamburger, P. Hebeisen, W. Löscher, D. Fabbro, P. Hillmann, M.P. Wymann, 4-(Difluoromethyl)-5-(4-((3R,5S)-3,5-dimethylmorpholino)-6-((R)-3-methylmorpholino)-1,3,5-triazin-2-yl)pyridin-2-amine (PQR626), a potent, orally available, and brain-penetrant mTOR inhibitor for the treatment of neurological disorders, J. Med. Chem. 63 (2020) 13595–13617.
[26] D. Rageot, T. Bohnacker, A. Melone, J.B. Langlois, C. Borsari, P. Hillmann, A. M. Sele, F. Beaufils, M. Zvelebil, P. Hebeisen, W. Loscher, J. Burke, D. Fabbro, M. P. Wymann, Discovery and preclinical characterization of 5-[4,6-Bis({3-oxa-8-azabicyclo[3.2.1]octan-8-yl})-1,3,5-triazin-2-yl]-4-(difluoro methyl)pyridin-2-amine (PQR620), a highly potent and selective mTORC1/2 inhibitor for cancer and neurological disorders, J. Med. Chem. 61 (2018) 10084–10105.
[27] J.C. Verheijen, K. Yu, L. Toral-Barza, I. Hollander, A. Zask, Discovery of 2-arylthieno[3,2-d]pyrimidines containing 8-oxa-3-azabi-cyclo[3.2.1]octane in the 4-position as potent inhibitors of mTOR with selectivity over PI3K, Bioorg. Med. Chem. Lett 20 (2010) 375–379.
[28] S. Bonazzi, C.P. Goold, A. Gray, N.M. Thomsen, J. Nunez, R.G. Karki, A. Gorde, J. D. Biag, H.A. Malik, Y. Sun, G. Liang, D. Lubicka, S. Salas, N. Labbe-Giguere, E. P. Keaney, S. McTighe, S. Liu, L. Deng, G. Piizzi, F. Lombardo, D. Burdette, J.-C. Dodart, C.J. Wilson, S. Peukert, D. Curtis, L.G. Hamann, L.O. Murphy, Discovery of a brain-penetrant ATP-competitive inhibitor of the mechanistic target of rapamycin (mTOR) for CNS disorders, J. Med. Chem. 63 (2020) 1068–1083.
[29] C. Borsari, D. Rageot, A. Dall'Asen, T. Bohnacker, A. Melone, A.M. Sele, E. Jackson, J.-B. Langlois, F. Beaufils, P. Hebeisen, D. Fabbro, P. Hillmann, M.P. Wymann, A conformational restriction strategy for the identification of a highly selective pyrimido-pyrrolo-oxazine mTOR inhibitor, J. Med. Chem. 62 (2019) 8609–8630.
[30] C. Borsari, E. Keles, A. Treyer, M. De Pascale, P. Hebeisen, M. Hamburger, M. P. Wymann, Second-generation tricyclic pyrimido-pyrrolo-oxazine mTOR inhibitor with predicted blood-brain barrier permeability, RSC Med. Chem. 12 (2021) 579–583.
[31] U. Stojiljkovic, C. Meyer, P. Boulay, P. Hebeisen, D. Rageot, M. Wymann, C. Borsari, Stereospecific synthesis of substituted sulfamidates as privileged morpholine building blocks, Synthesis (2022), https://doi.org/10.1055/a-1915-7794 [accepted manuscript].
[32] A. Zask, J. Kaplan, J.C. Verheijen, D.J. Richard, K. Curran, N. Brooijmans, E. M. Bennett, L. Toral-Barza, I. Hollander, S. Ayral-Kaloustian, K. Yu, Morpholine derivatives greatly enhance the selectivity of mammalian target of rapamycin (mTOR) inhibitors, J. Med. Chem. 52 (2009) 7942–7945.
[33] C. Brandt, P. Hillmann, A. Noack, K. Römermann, L.A. Öhler, D. Rageot, F. Beaufils, A. Melone, A.M. Sele, M.P. Wymann, D. Fabbro, W. Löscher, The novel, catalytic mTORC1/2 inhibitor PQR620 and the PI3K/mTORC1/2 inhibitor PQR530 effectively cross the blood-brain barrier and increase seizure threshold in a mouse model of chronic epilepsy, Neuropharmacology 140 (2018) 107–120.
[34] E. Singer, C. Walter, D. Fabbro, D. Rageot, F. Beaufils, M.P. Wymann, N. Rischert, O. Riess, P. Hillmann, H.P. Nguyen, Brain-penetrant PQR620 mTOR and PQR530 PI3K/mTOR inhibitor reduce huntingtin levels in cell models of HD, Neuropharmacology 162 (2020), 107812.
[35] W. Theilmann, B. Gericke, A. Schidlitzki, S.M. Muneeb Anjum, S. Borsdorf, T. Harries, S.L. Roberds, D.J. Aguiar, D. Brunner, S.C. Leiser, D. Song, D. Fabbro, P. Hillmann, M.P. Wymann, W. Löscher, Novel brain permeant mTORC1/2 inhibitors are as efficacious as rapamycin or everolimus in mouse models of acquired partial epilepsy and tuberous sclerosis complex, Neuropharmacology (2020), 108297.
[36] J.H. Zha, Y.C. Xia, C.L. Ye, Z. Hu, Q. Zhang, H. Xiao, B.T. Yu, W.H. Xu, G.Q. Xu, The anti-non-small cell lung cancer cell activity by a mTOR kinase inhibitor PQR620, Front. Oncol. 11 (2021), 669518.
[37] C. Tarantelli, E. Gaudio, P. Hillmann, F. Spriano, G. Sartori, L. Aresu, L. Cascione, D. Rageot, I. Kwee, F. Beaufils, E. Zucca, A. Stathis, M.P. Wymann, V. Cmiljanovic, D. Fabbro, F. Bertoni, The novel TORC1/2 kinase inhibitor PQR620 has anti-tumor activity in lymphomas as a single agent and in combination with venetoclax, Cancers 11 (2019) 775.
[38] A. Kumari, R.K. Singh, Morpholine as ubiquitous pharmacophore in medicinal chemistry: deep insight into the structure-activity relationship (SAR), Bioorg. Chem. 96 (2020), 103578.
[39] A. Venkanna, O.W. Kwon, S. Afzal, C. Jang, K.H. Cho, D.K. Yadav, K. Kim, H. G. Park, K.H. Chun, S.Y. Kim, M.H. Kim, Pharmacological use of a novel scaffold, anomeric N,N-diarylamino tetrahydropyran: molecular similarity search, chemocentric target profiling, and experimental evidence, Sci. Rep. 7 (2017), 12535.
[40] L. Fernández-Peña, C. Díez-Poza, P. González-Andrés, A. Barbero, The tetrahydrofuran motif in polyketide marine drugs, Mar. Drugs 20 (2022) 120.
[41] J. Kaplan, J.C. Verheijen, N. Brooijmans, L. Toral-Barza, I. Hollander, K. Yu, A. Zask, Discovery of 3,6-dihydro-2H-pyran as a morpholine replacement in 6-aryl-1H-pyrazolo[3,4-d]pyrimidines and 2-arylthieno[3,2-d]pyrimidines: ATP-competitive inhibitors of the mammalian target of rapamycin (mTOR), Bioorg. Med. Chem. Lett 20 (2010) 640–643.
[42] H. Hobbs, G. Bravi, I. Campbell, M. Convery, H. Davies, G. Inglis, S. Pal, S. Peace, J. Redmond, D. Summers, Discovery of 3-oxabicyclo[4.1.0]heptane, a non-nitrogen containing morpholine isostere, and its application in novel inhibitors of the PI3K-AKT-mTOR pathway, J. Med. Chem. 62 (2019) 6972–6984.
[43] T. Bohnacker, A.E. Prota, F. Beaufils, J.E. Burke, A. Melone, A.J. Inglis, D. Rageot, A.M. Sele, V. Cmiljanovic, N. Cmiljanovic, K. Bargsten, A. Aher, A. Akhmanova, J. F. Diaz, D. Fabbro, M. Zvelebil, R.L. Williams, M.O. Steinmetz, M.P. Wymann, Deconvolution of Buparlisib's mechanism of action defines specific PI3K and tubulin inhibitors for therapeutic intervention, Nat. Commun. 8 (2017), 14683.
[44] F. Beaufils, N. Cmiljanovic, V. Cmiljanovic, T. Bohnacker, A. Melone, R. Marone, E. Jackson, X. Zhang, A. Sele, C. Borsari, J. Mestan, P. Hebeisen, P. Hillmann, B. Giese, M. Zvelebil, D. Fabbro, R.L. Williams, D. Rageot, M.P. Wymann, 5-(4,6-Dimorpholino-1,3,5-triazin-2-yl)-4-(trifluoromethyl)pyridin-2-amine (PQR309), a potent, brain-penetrant, orally bioavailable, pan-class I PI3K/mTOR inhibitor as clinical candidate in oncology, J. Med. Chem. 60 (2017) 7524–7538.
[45] D.E. Clark, Rapid calculation of polar molecular surface area and its application to the prediction of transport phenomena. 2. Prediction of blood-brain barrier penetration, J. Pharmacol. Sci. 88 (1999) 815–821.
[46] J. Kelder, P.D. Grootenhuis, D.M. Bayada, L.P. Delbressine, J.P. Ploemen, Polar molecular surface as a dominating determinant for oral absorption and brain penetration of drugs, Pharm. Res. (N. Y.) 16 (1999) 1514–1519.
[47] C. Borsari, D. Rageot, F. Beaufils, T. Bohnacker, E. Keles, I. Buslov, A. Melone, A. M. Sele, P. Hebeisen, D. Fabbro, P. Hillmann, M.P. Wymann, Preclinical development of PQR514, a highly potent PI3K inhibitor bearing a difluoromethyl-pyrimidine moiety, ACS Med. Chem. Lett. 10 (2019) 1473–1479.
[48] D.J. Richard, J.C. Verheijen, K. Yu, A. Zask, Triazines incorporating (R)-3-methylmorpholine are potent inhibitors of the mammalian target of rapamycin

(mTOR) with selectivity over PI3Kalpha, Bioorg. Med. Chem. Lett 20 (2010) 2654–2657.
[49] D. Rageot, T. Bohnacker, E. Keles, J.A. McPhail, R.M. Hoffmann, A. Melone, C. Borsari, R. Sriramaratnam, A.M. Sele, F. Beaufils, P. Hebeisen, D. Fabbro, P. Hillmann, J.E. Burke, M.P. Wymann, (S)-4-(Difluoromethyl)-5-(4-(3-methylmorpholino)-6-morpholino-1,3,5-triazin-2-yl)pyridin-2-amine (PQR530), a potent, orally bioavailable, and brain-penetrable dual inhibitor of class I PI3K and mTOR kinase, J. Med. Chem. 62 (2019) 6241–6261.
[50] A.M. Venkatesan, Z. Chen, O.D. Santos, C. Dehnhardt, E.D. Santos, S. Ayral-Kaloustian, R. Mallon, I. Hollander, L. Feldberg, J. Lucas, K. Yu, I. Chaudhary, T. S. Mansour, PKI-179: an orally efficacious dual phosphatidylinositol-3-kinase (PI3K)/mammalian target of rapamycin (mTOR) inhibitor, Bioorg. Med. Chem. Lett 20 (2010) 5869–5873.
[51] C. Borsari, E. Keles, J.A. McPhail, A. Schaefer, R. Sriramaratnam, W. Goch, T. Schaefer, M. De Pascale, W. Bal, M. Gstaiger, J.E. Burke, M.P. Wymann, Covalent proximity scanning of a distal cysteine to target PI3Kα, J. Am. Chem. Soc. 144 (2022) 6326–6342.
[52] H. Yang, D.G. Rudge, J.D. Koos, B. Vaidialingam, H.J. Yang, N.P. Pavletich, mTOR kinase structure, mechanism and regulation, Nature 497 (2013) 217–223.
[53] P.A. Wood, F.H. Allen, E. Pidcock, Hydrogen-bond directionality at the donor H atom—analysis of interaction energies and database statistics, CrystEngComm 11 (2009) 1563–1571.
[54] J.A. McPhail, J.E. Burke, Drugging the phosphoinositide 3-kinase (PI3K) and phosphatidylinositol 4-kinase (PI4K) family of enzymes for treatment of cancer, immune disorders, and viral/parasitic infections, Adv. Exp. Med. Biol. 1274 (2020) 203–222.
[55] C.W. McNamara, M.C. Lee, C.S. Lim, S.H. Lim, J. Roland, O. Simon, B.K. Yeung, A. K. Chatterjee, S.L. McCormack, M.J. Manary, A.M. Zeeman, K.J. Dechering, T. S. Kumar, P.P. Henrich, K. Gagaring, M. Ibanez, N. Kato, K.L. Kuhen, C. Fischli, A. Nagle, M. Rottmann, D.M. Plouffe, B. Bursulaya, S. Meister, L. Rameh, J. Trappe, D. Haasen, M. Timmerman, R.W. Sauerwein, R. Suwanarusk, B. Russell, L. Renia, F. Nosten, D.C. Tully, C.H. Kocken, R.J. Glynne, C. Bodenreider, D.A. Fidock, T. T. Diagana, E.A. Winzeler, Targeting Plasmodium PI(4)K to eliminate malaria, Nature 504 (2013) 248–253.
[56] U.H. Manjunatha, S. Vinayak, J.A. Zambriski, A.T. Chao, T. Sy, C.G. Noble, G.M. C. Bonamy, R.R. Kondreddi, B. Zou, P. Gedeck, C.F. Brooks, G.T. Herbert, A. Sateriale, J. Tandel, S. Noh, S.B. Lakshminarayana, S.H. Lim, L.B. Goodman, C. Bodenreider, G. Feng, L. Zhang, F. Blasco, J. Wagner, F.J. Leong, B. Striepen, T. T. Diagana, A Cryptosporidium PI(4)K inhibitor is a drug candidate for cryptosporidiosis, Nature 546 (2017) 376–380.
[57] J. Reuberson, H. Horsley, R.J. Franklin, D. Ford, J. Neuss, D. Brookings, Q. Huang, B. Vanderhoydonck, L.J. Gao, M.Y. Jang, P. Herdewijn, A. Ghawalkar, F. Fallah-Arani, A.R. Khan, J. Henshall, M. Jairaj, S. Malcolm, E. Ward, L. Shuttleworth, Y. Lin, S. Li, T. Louat, M. Waer, J. Herman, A. Payne, T. Ceska, C. Doyle, W. Pitt, M. Calmiano, M. Augustin, S. Steinbacher, A. Lammens, R. Allen, Discovery of a potent, orally bioavailable PI4KIIIβ inhibitor (UCB9608) able to significantly prolong allogeneic organ engraftment in vivo, J. Med. Chem. 61 (2018) 6705–6723.
[58] B.D. Hopkins, C. Pauli, X. Du, D.G. Wang, X. Li, D. Wu, S.C. Amadiume, M. D. Goncalves, C. Hodakoski, M.R. Lundquist, R. Bareja, Y. Ma, E.M. Harris, A. Sboner, H. Beltran, M.A. Rubin, S. Mukherjee, L.C. Cantley, Suppression of insulin feedback enhances the efficacy of PI3K inhibitors, Nature 560 (2018) 499–503.
[59] K.C. Wood, J.S. Gutkind, Challenges and emerging opportunities for targeting mTOR in cancer, Cancer Res. 82 (2022) 3884–3887.
[60] C. Tarantelli, A. Lupia, A. Stathis, F. Bertoni, Is there a role for dual PI3K/mTOR inhibitors for patients affected with lymphoma? Int. J. Mol. Sci. 21 (2020) 1060.
[61] A. Conconi, M. Raderer, S. Franceschetti, L. Devizzi, A.J. Ferreri, M. Magagnoli, L. Arcaini, P.L. Zinzani, G. Martinelli, U. Vitolo, B. Kiesewetter, E. Porro, A. Stathis, G. Gaidano, F. Cavalli, E. Zucca, Clinical activity of everolimus in relapsed/refractory marginal zone B-cell lymphomas: results of a phase II study of the International Extranodal Lymphoma Study Group, Br. J. Haematol. 166 (2014) 69–76.
[62] C. Tarantelli, E. Gaudio, A.J. Arribas, I. Kwee, P. Hillmann, A. Rinaldi, L. Cascione, F. Spriano, E. Bernasconi, F. Guidetti, L. Carrassa, R.B. Pittau, F. Beaufils, R. Ritschard, D. Rageot, A. Sele, B. Dossena, F.M. Rossi, A. Zucchetto, M. Taborelli, V. Gattei, D. Rossi, A. Stathis, G. Stussi, M. Broggini, M.P. Wymann, A. Wicki, E. Zucca, V. Cmiljanovic, D. Fabbro, F. Bertoni, PQR309 is a novel dual PI3K/mTOR inhibitor with preclinical antitumor activity in lymphomas as a single agent and in combination therapy, Clin. Cancer Res. 24 (2018) 120–129.
[63] P. Klener, D. Sovilj, N. Renesova, L. Andera, BH3 mimetics in hematologic malignancies, Int. J. Mol. Sci. 22 (2021), 10157.
[64] M.S. Davids, A.W. Roberts, V.P. Kenkre, W.G. Wierda, A. Kumar, T.J. Kipps, M. Boyer, A.H. Salem, J.C. Pesko, J.A. Arzt, M. Mantas, S.Y. Kim, J.F. Seymour, Long-term follow-up of patients with relapsed or refractory non-hodgkin lymphoma treated with venetoclax in a phase I, first-in-human study, Clin. Cancer Res. 27 (2021) 4690–4695.
[65] D. Rageot, F. Beaufils, C. Borsari, A. Dall'Asen, M. Neuburger, P. Hebeisen, M. P. Wymann, Scalable, economical, and practical synthesis of 4-(difluoromethyl) pyridin-2-amine, a key intermediate for lipid kinase inhibitors, Org. Process Res. Dev. 23 (2019) 2416–2424.
[66] L. Palatinus, G. Chapuis, SUPERFLIP– a computer program for the solution of crystal structures by charge flipping in arbitrary dimensions, J. Appl. Crystallogr. 40 (2007) 786–790.
[67] L. Palatinus, S.J. Prathapa, S. van Smaalen, EDMA: a computer program for topological analysis of discrete electron densities, J. Appl. Crystallogr. 45 (2012) 575–580.
[68] O.V. Dolomanov, L.J. Bourhis, R.J. Gildea, J.A.K. Howard, H. Puschmann, OLEX2: a complete structure solution, refinement and analysis program, J. Appl. Crystallogr. 42 (2009) 339–341.
[69] G.M. Sheldrick, Crystal structure refinement with SHELXL, Acta Crystallogr C Struct Chem 71 (2015) 3–8.
[70] C.F. Macrae, I. Sovago, S.J. Cottrell, P.T.A. Galek, P. McCabe, E. Pidcock, M. Platings, G.P. Shields, J.S. Stevens, M. Towler, P.A. Wood, Mercury 4.0: from visualization to analysis, design and prediction, J. Appl. Crystallogr. 53 (2020) 226–235.
[71] M.A. Fabian, W.H. Biggs 3rd, D.K. Treiber, C.E. Atteridge, M.D. Azimioara, M. G. Benedetti, T.A. Carter, P. Ciceri, P.T. Edeen, M. Floyd, J.M. Ford, M. Galvin, J. L. Gerlach, R.M. Grotzfeld, S. Herrgard, D.E. Insko, M.A. Insko, A.G. Lai, J. M. Lelias, S.A. Mehta, Z.V. Milanov, A.M. Velasco, L.M. Wodicka, H.K. Patel, P. P. Zarrinkar, D.J. Lockhart, A small molecule-kinase interaction map for clinical kinase inhibitors, Nat. Biotechnol. 23 (2005) 329–336.
[72] M.W. Karaman, S. Herrgard, D.K. Treiber, P. Gallant, C.E. Atteridge, B.T. Campbell, K.W. Chan, P. Ciceri, M.I. Davis, P.T. Edeen, R. Faraoni, M. Floyd, J.P. Hunt, D. J. Lockhart, Z.V. Milanov, M.J. Morrison, G. Pallares, H.K. Patel, S. Pritchard, L. M. Wodicka, P.P. Zarrinkar, A quantitative analysis of kinase inhibitor selectivity, Nat. Biotechnol. 26 (2008) 127–132.